

2017

Non-Aqueous Phase Liquid Transport and Dynamics in Simulated Karst Conduits

Samuel Noah Jacobson

Bucknell University, snj003@bucknell.edu

Follow this and additional works at: https://digitalcommons.bucknell.edu/honors_theses

Recommended Citation

Jacobson, Samuel Noah, "Non-Aqueous Phase Liquid Transport and Dynamics in Simulated Karst Conduits" (2017). *Honors Theses*. 423.

https://digitalcommons.bucknell.edu/honors_theses/423

This Honors Thesis is brought to you for free and open access by the Student Theses at Bucknell Digital Commons. It has been accepted for inclusion in Honors Theses by an authorized administrator of Bucknell Digital Commons. For more information, please contact dcadmin@bucknell.edu.

Non-Aqueous Phase Liquid Transport and Dynamics in Simulated Karst Conduits

by

Samuel N. Jacobson

Submitted to the Honors Council

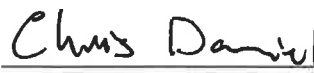
For Honors in Geology & Environmental Geosciences

April 12, 2017

Approved by:



Adviser: Ellen Herman



Department Chair: Chris Daniel

Acknowledgements

I would like to acknowledge the following people for their roles in creating this project and making it a success. First and foremost this project would not have been possible without Ellen Herman acting as a guiding force through project conceptualization. More than just providing critical feedback during the writing process, and a grounding in the basics of fluid flow she opened my eyes to the possibilities of research. Thanks to Dorothy Vesper at West Virginia University for connecting resources and bouncing ideas and future plans about the project. Thanks also to Johnathan Moore and Dustin Crandall and the National Energy Technology Labs in Morgantown for conducting the imaging and serving as resource for the XRCT part of the process. Thanks to Jeff Trop, Mary Beth Gray, Craig Kochel, and Chris Daniel for providing feedback on oral presentations and helping to talk through issues faced during the project and for constituting the Bucknell University geology department. Thanks to Carilee Dill and Brad Jordan make the Geology department run and without them this project would have been dead before it started. Thanks to Brian Smith and Rob Jacob for serving as my honors committee and for providing many revisions. Thanks also to the McKenna foundation for funding this summer research and the Dalal Family for funding research during the academic year. This project would not have succeeded without the emotional and moral support of the fellow geology majors, their input and the social hours in O'Leary 105.

Of course none of this would have been possible without my mother and father, inspiring a questioning kid to push further.

Table of Contents

Abstract.....	1
Introduction.....	2
Project Overview.....	3
Physical System.....	4
Karst.....	4
Non-Aqueous Phase Liquids.....	9
Hydrogel Beads.....	14
Flow Cell.....	16
3-D Printing.....	16
Imaging.....	20
Methods.....	21
Digital Design.....	22
Printing Techniques Overview	26
Acetone Treatment.....	27
Permeability Assessment.....	29
FFF of Conduits.....	31
Construction.....	33
Flow Components.....	35
Imaging.....	35
Flow Test.....	38
Results and Discussion.....	38
Flow System.....	38
XRCT Data.....	40
Further Research.....	44
Conclusion.....	46
Bibliography.....	53

List of Tables

Table 1: Complete list of parameters used in Simplify3D program.....48

List of Figures	
Figure 1 - Karst Block Diagram.....	4
Figure 2 – Cave Geometries and their causes.....	5
Figure 3 – Map of karst potential karst and potential water soluble rock across the continental United States.....	6
Figure 4 – Triple porosity block models.....	8
Figure 5 – Cartoon of LNPL migration through the subsurface.....	10
Figure 6 – Cartoon of DNAPL migration through the subsurface.....	12
Figure 7 – Conceptual model of DNAPL movement through karst system.....	14
Figure 8 – Diagram of Sterolithography (SLA) technique.....	16
Figure 9 – Diagram of Fused Filament Fabrication (FFF) technique.....	17
Figure 10 – Diagram of Selective Laser Sintering (SLA) technique.....	19
Figure 11 – Simplified diagram of XRCT imaging process.....	21
Figure 12 – Series of images showing digital model construction on Solidworks.....	23
Figure 13 – Photo of post-hole joining system.....	25
Figure 14 – Photo of acetone vapor treatment chamber.....	28
Figure 15 – Photo of cups used to evaluate ability to hold water.....	30
Figure 16 – Photo of assembled core.....	33
Figure 17 – Photo of assembled core with inflow and outflow tubes attached.....	34
Figure 18 – Diagram of Hessler-style core holder.....	35
Figure 19 – Cartoon of XRCT scanner.....	36
Figure 20 – Cartoon of X-ray beam and sample.....	37
Figure 21 – Photograph of completed core.....	39
Figure 22 – Composite XRCT image.....	41
Figure 23 – Cross section XRCT image series.....	42
Figure 24 – Plan view XRCT image series.....	43

Abstract

Flow and contaminant transport in karstic aquifers differs drastically from porous media. Little work has been done to quantify the transport dynamics of non-aqueous phase liquids (NAPLs) in karst in the lab. Some studies have 3-D printed fractures to evaluate multiphase transport at the core scale, but examination of conduit flow using this technique is lacking in the literature.

This project illustrates some of the strengths and limitations of 3-D printing and using X-ray computed tomography (XRCT) to characterize flow. After testing prints made from stereolithographic resin (SLA) and polyactic acid (PLA) plastic, we decided to use acrylonitrile butadiene styrene (ABS) plastic to construct flow cells to image turbulent water-NAPL-analog flow in conduits using XRCT. To mimic conduit flow transport dynamics, printed conduit apertures are elliptical and measure more than 1 cm in cross sectional area to promote turbulent flow.

Fused filament fabrication, a type of 3-D printing process used during construction, produces permeable prints. To minimize communication between the conduit and surrounding support matrix allowing reuse of flow cells, we moderately melted cores using acetone vapor. This allows dissolved plastic to fill and harden between layers making the walls impermeable.

Flow of water and hydrogel beads, a potential non-toxic NAPL analog tracer candidate, was imaged with a modified XRCT scanner. XRCT images were stitched

together to identify conduit irregularities, and to image beads as they move through the conduit. Future work aims to develop hydrogel beads that behave like NAPLs in the lab.

As a novel technique in karst modeling, printing and imaging requires further validation. Our images do not differentiate between beads, epoxy, and plastic, making validation difficult. Future work should involve radiologic agents added to water and NAPL-analogs during experimentation to increase the contrast between water and hydrogel beads in order to clarify flow paths.

Introduction

In an industrial society, chemical spills and contamination of water are inevitable. Designing the best containers and resilient systems are admirable proactive measures; however those systems will inevitably fail. Remedying that failure by understanding subsurface chemical movement and remediation strategies is a key component of industrial chemical use. Before a spill can be remediated the plume has to be characterized so the remediation can be targeted. Plumes are dependent on the material spilled, material through which it is moving, and local conditions.

This project focuses on a specific terrain type, karst, for its unique permeability and the transport of non-aqueous phase liquids (NAPLs) through karst. NAPLs are only partially soluble in water, and thus cannot be traced using a traditional conservative tracer. Tracers are chemicals that can be released in a natural system in a known quantity at a specific location and then detected elsewhere. A tracer can provide site specific information including the flow rate of water, and in the event of contamination can be

used to model the extent of contamination. NAPL movement through a system is not the same as water, so it is difficult to model accurately. Especially because karst is so variable, relying on lab data for residence time and remediation required is risky.

Releasing a non-toxic tracer that behaves like a NAPL would provide useful field data on the severity of a contamination event. Before a tracer can be deployed in a natural system at a field site, it must be proven to behave as a NAPL in a controlled setting.

Project Overview

This project aims to manufacture flow cells that bridge the knowledge gap between theory of NAPL transport and field studies. Darcian NAPL transport through porous material is well understood. This project focuses on NAPL transport in karst conduits because flow in conduits is non-Darcian. Literature is sparse concerning any turbulent NAPL transport, much less complex karst triple porosity systems. To understand turbulent NAPL transport and storage, we must construct our own system and assess it. These flow cells will promote turbulent flow in conduits. Water and NAPL-analogs both flow through custom, 3-D printed bench scale conduit analogues designed to encourage turbulent flow and mimic basic conduit geometries. Water-NAPL two phase flow will be imaged using X-ray computed tomography. Once turbulent NAPL transport is understood, NAPL-analog tracers can be manufactured which will lead to more effective site assessment of NAPL contamination. This information may be used to verify conceptual models and for future development of a suite of tracers for use to mimic NAPLs in natural karst systems.

Physical system

Karst

The term karst is applied to terrains where the underlying bedrock is composed of water-soluble rock. Water infiltrating karst regions dissolves rock along preferential flow paths.

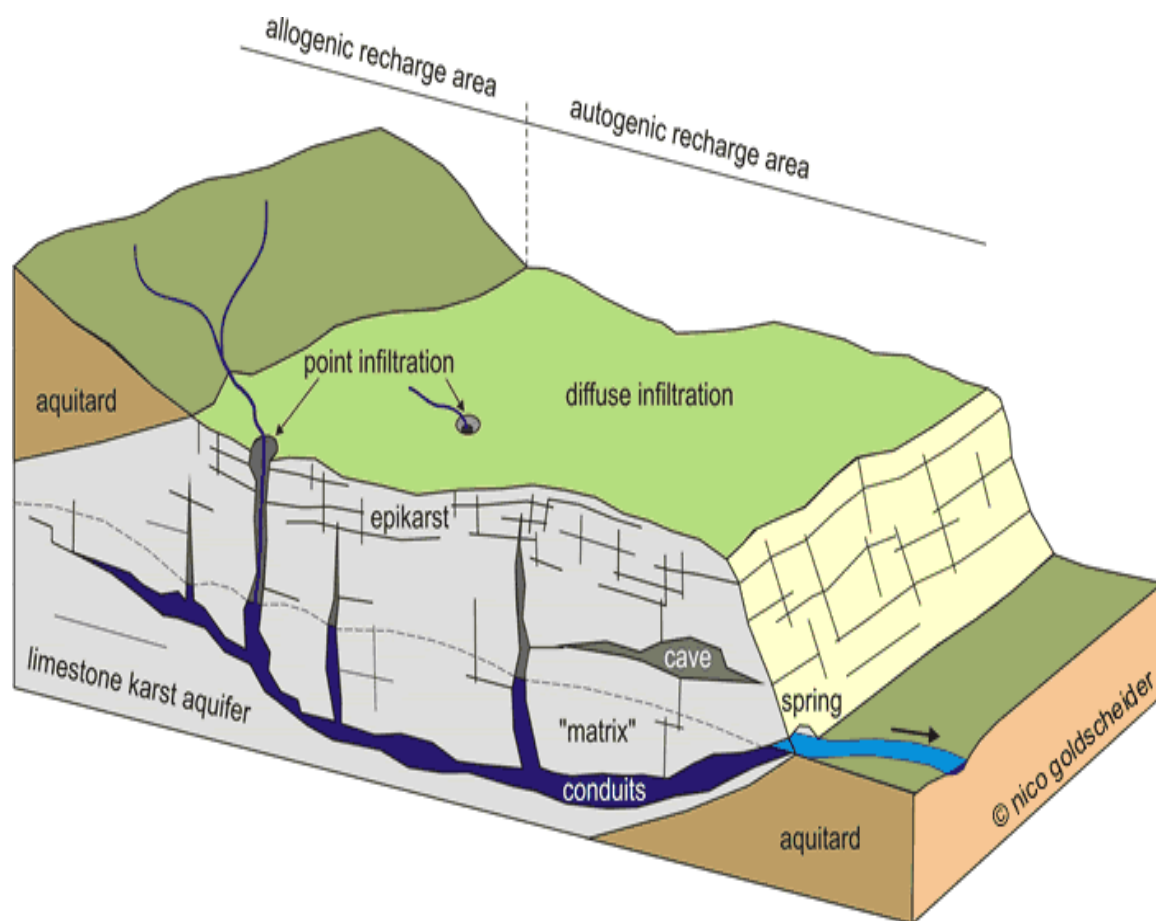


Figure 1 – Simplified block diagram of karst system. This project focuses on conduit flow depicted in the base of the cross section (Goldscheider and Drew 2007)













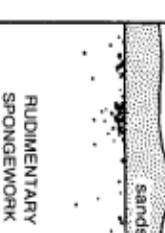
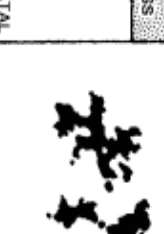


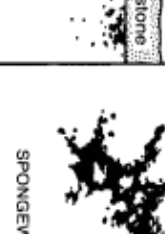




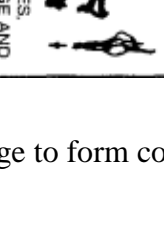


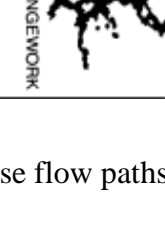



		TYPE OF RECHARGE				
		VIA KARST DEPRESSIONS		DIFFUSE		HYPOGENIC
DOMINANT TYPE OF POROSITY		INTERGRANULAR	BEDDING PARTINGS	FRACTURES		
SINKHOLES (LIMITED DISCHARGE FLUCTUATION)	BRANCHWORKS (USUALLY SEVERAL LEVELS) & SINGLE PASSAGES					THROUGH SANDSTONE MOST CAVES ENLARGED FURTHER BY RECHARGE FROM OTHER SOURCES
						
SINKING STREAMS (GREAT DISCHARGE FLUCTUATION)	SINGLE PASSAGES AND CRUDE BRANCHWORKS, USUALLY WITH THE FOLLOWING FEATURES SUPERIMPOSED:					INTO POROUS SOLUBLE ROCK MOST CAVES FORMED BY MIXING AT DEPTH
						DISSOLUTION BY ACIDS OR DEEP-SEATED SOURCE OR BY COOLING OF THERMAL WATER
						
						
						

Figure 2 – Grid from Palmer (1991) showing the different geometric classification of caves and how they are formed. Conduits in this thesis are not meant to simulate all cave types. This work focuses on the conduits developed via karst depressions.

Over time, these flow paths enlarge to form conduits, essentially underground pipes (Figure 1).

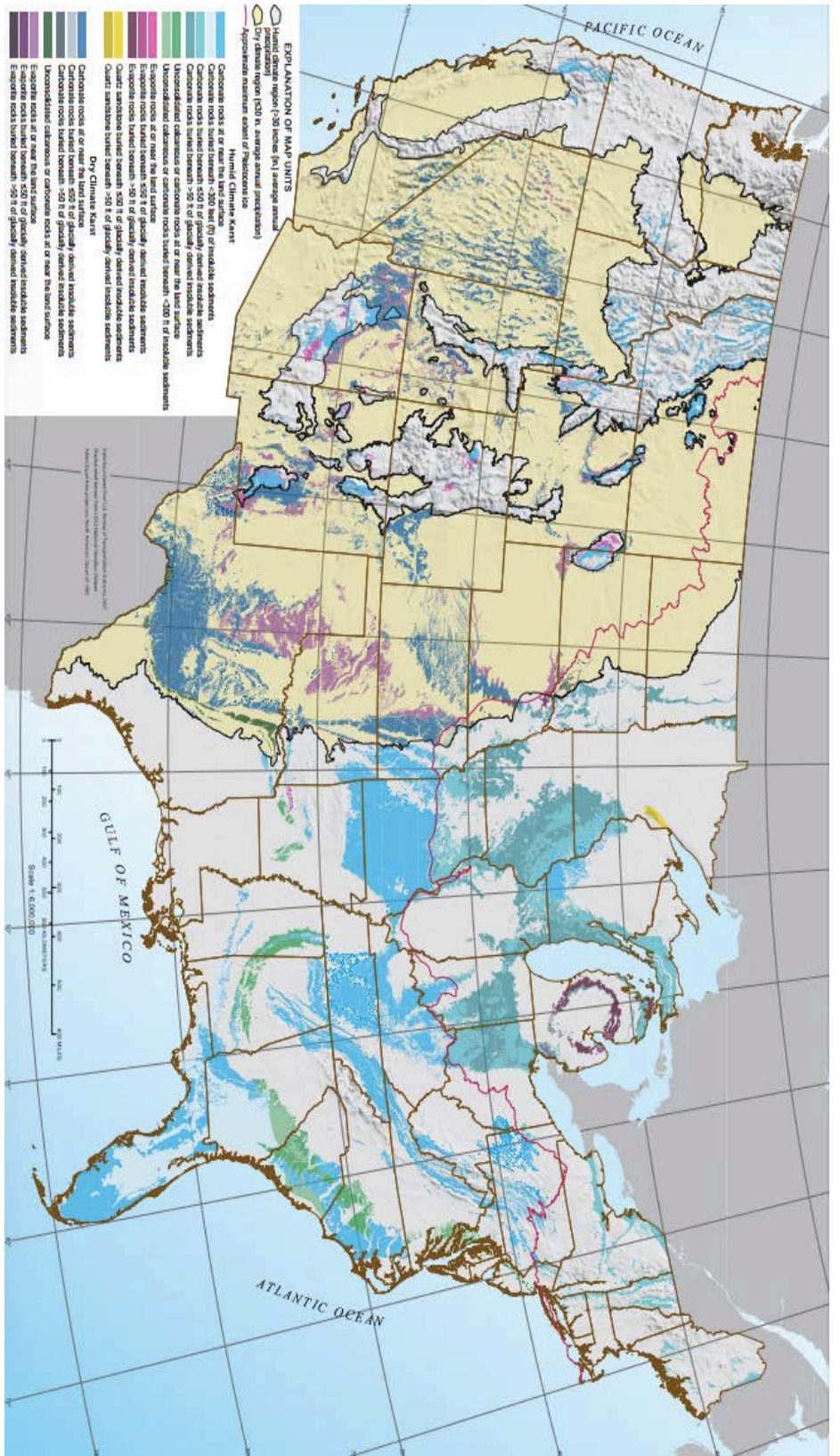


Figure 3 – Map of karst and potential karst in water soluble rocks across the continental United States showing the wide distribution and variety of karst (Weary and Doctor 2014).

Conduits can take many different shapes depending on the recharge rate of water, solutional aggressiveness of the water, preexisting fractures in the bedrock, and other variables (Figure 2) (Palmer 1991). Palmer (1991) showed that karst systems under similar conditions develop similar morphologies. These morphologies form the bedrock for developing simulated conduits in this project.

Karst is widespread across the United States, constituting 20% of the land surface in the country (Figure 3) (USGS). According to the US Geological Survey (USGS), roughly 40% of the groundwater used for drinking in the United States comes from karstic aquifers (USGS Office of Groundwater). Thus understanding contaminant transport in karstic aquifers serves both applied and basic research goals.

Aquifers can be categorized by the hydraulic conductivity of their constituent members, the ease with which water moves through them. Porous media, including sands, clays, and sandstones, are areas where water moves relatively slowly through pore spaces in the subsurface. This movement of water, when it occurs in karst, is called matrix flow and is on the order of centimeters per day (Loop and White 2001). Porous media is often modeled as isotropic, homogeneous, and dominated by laminar flow.

Rock that has been stressed and fractured can have water flowing through those fractures, termed fracture flow. This rock most likely exhibits a combination of matrix and fracture flow. Fractures increase the permeability of the rock and tend to dominate the overall hydraulic conductivity of the system. Fractures are created through a mechanical process and are therefore independent of a rock's solubility.

Karst, the landform created by water soluble rock, can contain matrix, fracture, and conduit flow making it strongly anisotropic. This classification system and communication between the three types of flow is described by the triple porosity model (Worthington 1999) (Figure 4). Fractures and conduits both are orders of magnitude more

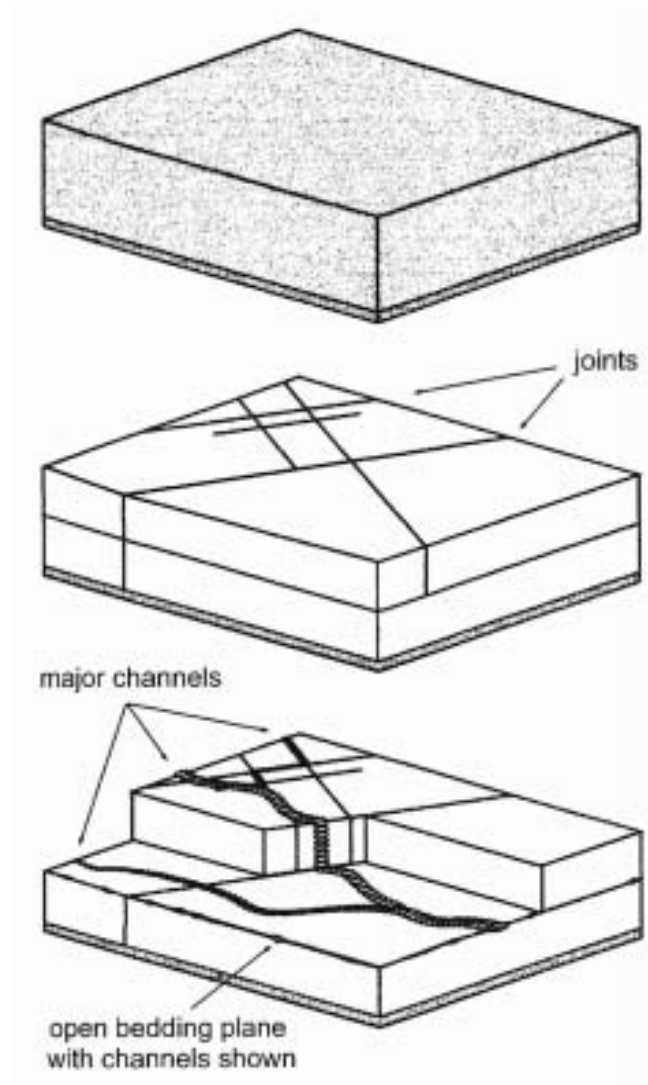


Figure 4 - Block diagram showing different porosity types: matrix porosity (top), fracture and matrix porosity (middle), conduit, fracture, and matrix porosity (bottom) (Worthington 1999).

hydraulically conductive than matrix flow (Worthington et al. 2000). Conduits are solutionally enlarged features that often grow along fractures, bed plane partings, or other preexisting flow paths (Palmer 1991). Conduit flow is strictly associated with karst, is characterized by turbulent flow, and can flow on the order of kilometers per day, exceeding flow rates associated with fracture flow and surface water (Loop and White 2001). Cross-sectional area of the conduit has a significant impact on the transition to turbulence. White (2002) identifies the transition to turbulence commonly occurring around apertures one centimeter or greater. Overall, these three sources of porosity combine to move water more quickly through karst than porous media under similar hydraulic gradients.

Non-Aqueous Phase Liquids (NAPLs)

Non-Aqueous phase liquids (NAPLs) are a class of chemicals that are only slightly miscible in water and often hazardous to humans. Most NAPLs have significant potential to contaminate aquifers due to their widespread usage. Their differing densities and miscibility in water affect their behavior and transport through aquifers. They are divided into two categories based on their density in relation to water: light NAPLs (LNAPLs) and dense NAPLs (DNAPLs). Gasoline is a well-known LNAPL, and chlorinated solvents such as carbon tetrachloride and trichloroethylene used as degreasers, paint thinners, and cleaning solutions are common examples of DNAPLs. Their low solubility means that a single spill can contaminate significant amounts of water, as the contaminant is not necessarily transported through the system with the water but remains as a continuing source of contamination through long-term slow dissolution (Figure 5).

DNAPLs tend to collect and pool at stratigraphic lows along impermeable boundaries while LNAPLs collect near the top of the water column.

NAPL transport studies have focused on laminar flow through porous media.

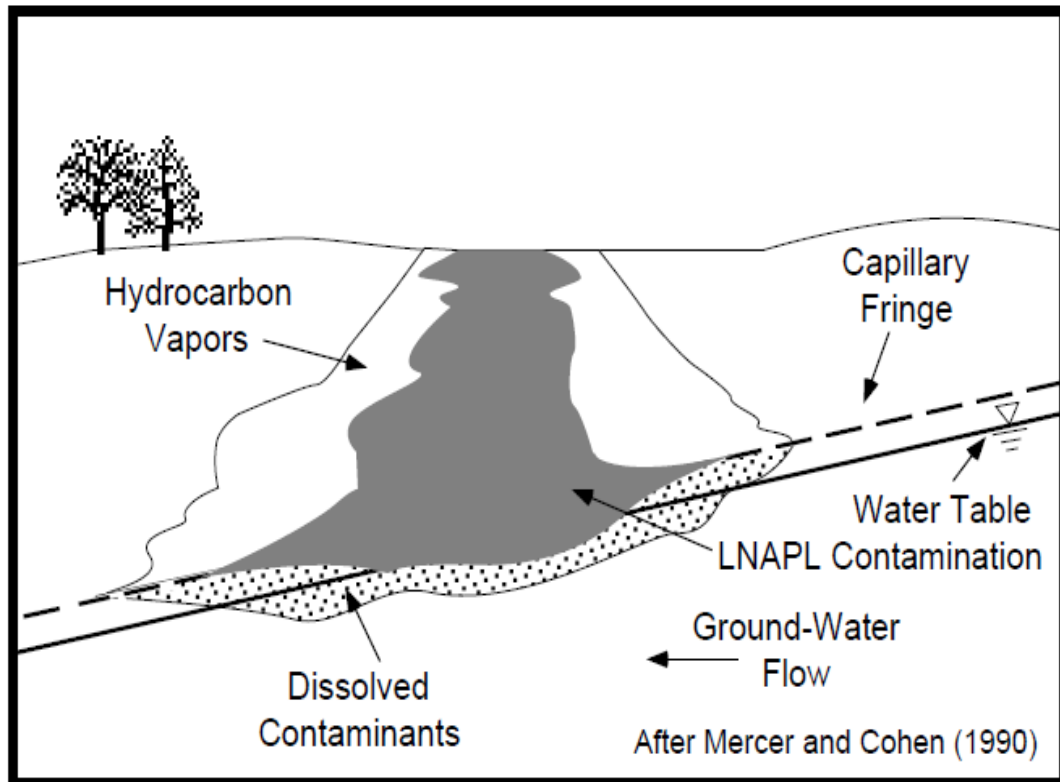


Figure 5 – Cartoon illustrating LNAPL movement through a porous medium. LNAPL tends to stay at or near the water table and extend in a plume parallel to groundwater flow, though the plume can move along the impermeable contact against groundwater flow. LNAPLs enter the phreatic zone only through dissolution into groundwater (Newell et al. 1995).

Some studies are conducted as column experiments in the lab (e.g., Russo et al. 2009a; Russo et al. 2009b). Other researchers prefer to work with contaminated sites and characterize movement of NAPLs in the subsurface (e.g., Holzmer et al. 2005; Jakobsen and Knud 1999). Still others image pore scale interactions in controlled laboratory settings (e.g., Becker et al. 2003).

Because the NAPLs are a wide ranging class of chemicals, each chemical's relevant physical properties must be understood to facilitate remediation (e.g., Newell et al. 1995; Huling and Weaver 1991). There exists a rich body of work detailing effective methods of remediating NAPL-contaminated sites but again this work is largely limited to porous media. McCray et al. (2011) for example detail various remediation techniques and their effectiveness working with NAPLS from a typical porous media dominated aquifer in Dover. US EPA standards for remediation and further reading can be found in Newell et al. (1995) and Huling and Weaver (1991). Robust mathematical models have also been offered for NAPL flow in porous media (e.g., Huyakorn 1994). There exists limited research on NAPL movement through fracture and conduit dominated terrain. Jancin and Ebaugh (2002) for example have conducted a case study of a DNAPL plume moving through karst bedrock. These types of non-porous contamination studies are atypical and do not receive much attention in the literature.

Surface and conduit flow share some similarities like turbulent dynamics, but there has not been much research describing the dynamics of NAPL behavior in either surface or karst conduit waters. In laminar flow regimes NAPL plumes move through connected pore spaces (matrix flow), driven by gravity. Migration patterns depend on amount of product released, porosity of material, homogeneity of material, and type of

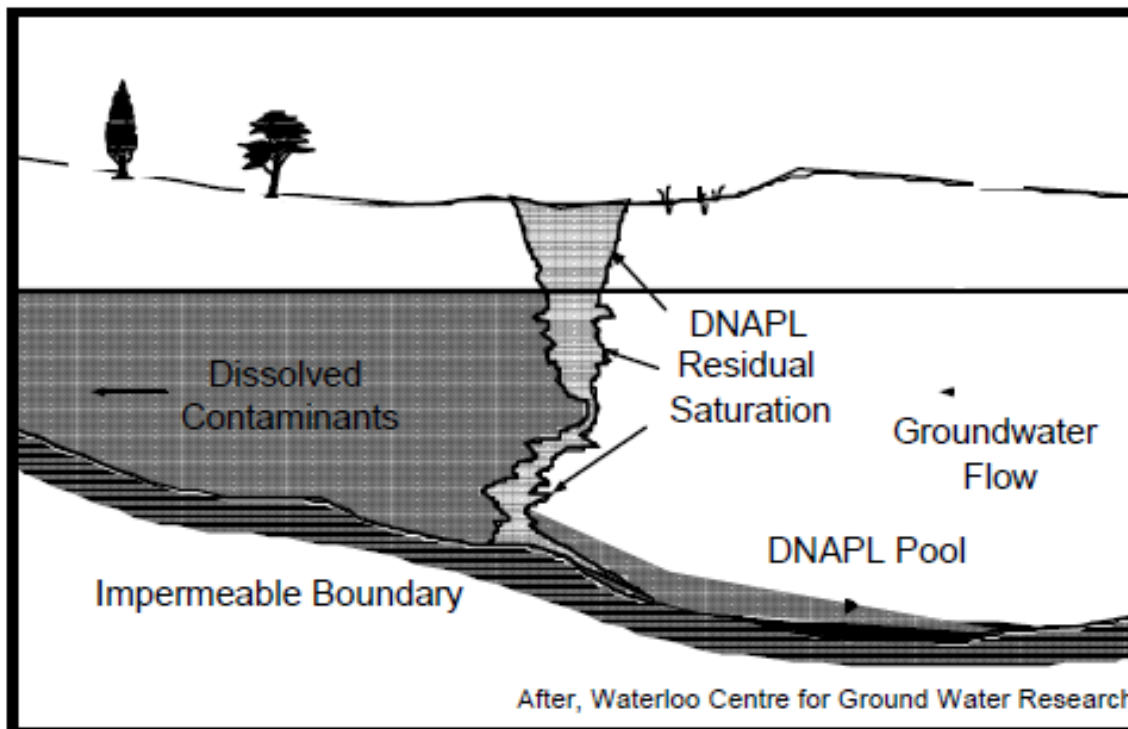


Figure 6 – Cartoon illustrating DNAPL movement through a porous medium and pooling along an impermeable boundary. DNAPL can penetrate the water table and extend in a plume parallel to groundwater flow, though the plume can move along the impermeable contact against groundwater flow to a topographic low. The DNAPL pool will continue to contaminate water over time (Huling and Weaver 1991).

NAPL released. LNAPL tends to pool along the capillary fringe and spread along the contact, as it ‘floats’ on groundwater (Figure 5). DNAPL alternatively, driven by density contrast between DNAPL and water, tends to migrate vertically until there is insufficient pressure from overlying DNAPL to push into lower pores (Huling and Weaver 1991) (Figure 6). At an impermeable boundary, DNAPL will pool and can continue to

contaminate surrounding groundwater as it flows past. Given that NAPLs encompass a variety of different chemicals with different interactions to soil and rock grains, some NAPLs will sorb onto soil grains, while others will flow with groundwater through connected pore spaces (Soga et al. 2004). Though NAPLs are a heterogeneous class of chemicals, in terms of their movement through porous media, underlying Darcian flow forms the basis of modeling their movement through the matrix. Loop and White forward a conceptual model of DNAPL movement in and through a karst system (Figure 7) (Loop and White 2001). In their model there are multiple paths into the conduit system, through the epikarst, karst windows, and sinkholes. Some of the NAPL will be stored in the epikarst and soil; in this part of the model, flow can be considered laminar and slow. Water-NAPL mixtures flowing through sinkholes or karst windows may be moving as free surface or pipe-full turbulent flow. Once the NAPL penetrates the surface and enters the conduit system, the turbulent flow regime governs. NAPL can be trapped by sediment in the conduit, in relict passages, and in deep storage. Over time the NAPL will dissolve, flow out of the system at streams and springs, or shift to deep storage. Degradation often comes at the expense of contaminating groundwater.

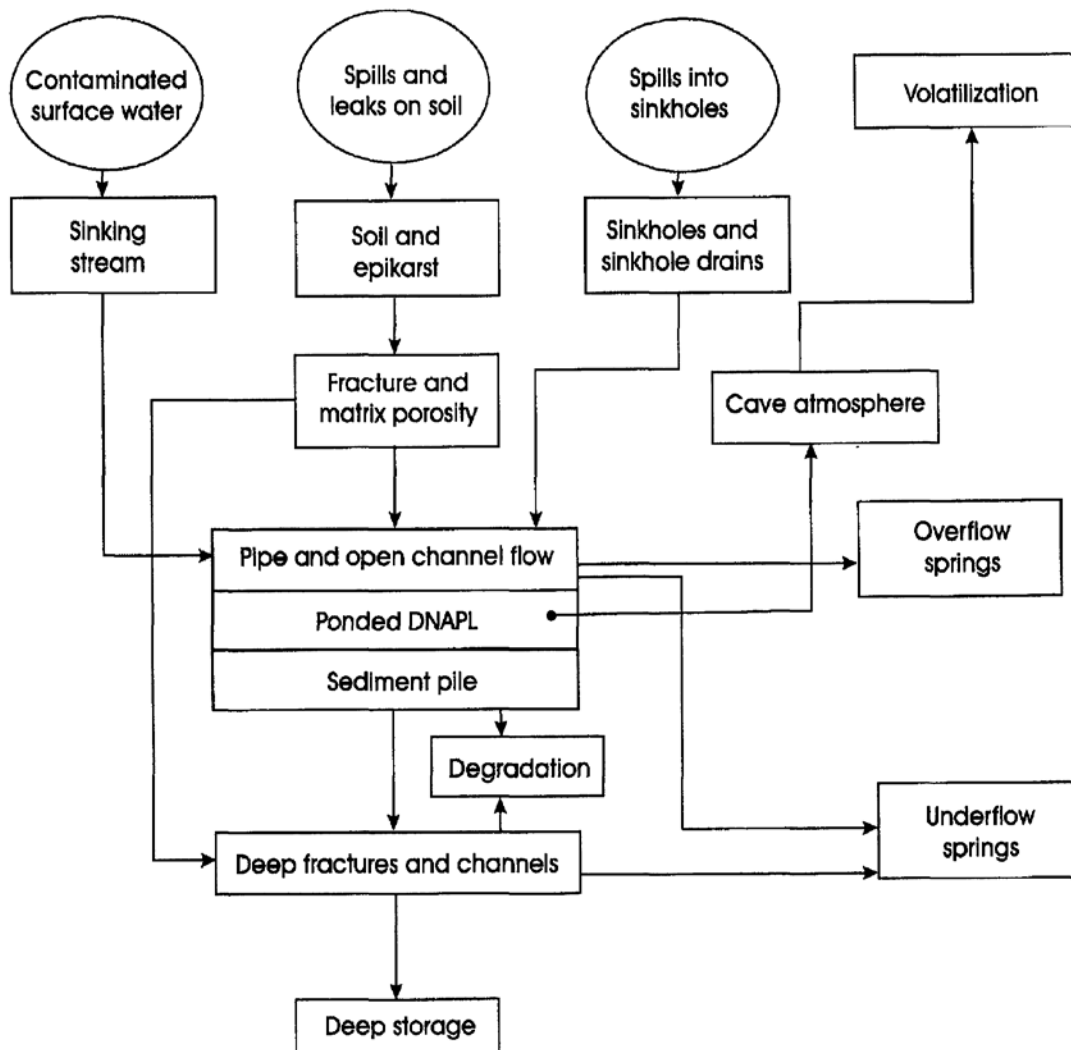


Figure 7 – Conceptual model of DNAPL in karst. This project seeks to model the central box, pipe and open channel flow. DNAPL enters the subsurface through the circles at the top of the diagram, travels to different boxes along arrow connections, and settles in one of the outermost boxes (Loop and White 2001).

Hydrogel Beads

This project is part of an overall project to develop tracers that behave similarly to NAPLs in turbulent flow. NAPLs tend to be toxic and therefore cannot be ethically

released into the environment for the purposes of academic study. An ideal developed tracer has to be non-toxic and detectable if released into the field. Traditional tracers like Rhodamine-WT, lithium, and bromide are conservative and highly soluble and are used to establish flow paths, flow velocities, residence times, plume migration for certain contaminants, and other characteristics of aquifers (Dierberg and DeBusk 2005). Recall that NAPLs are only slightly soluble and either float or sink beneath groundwater. This negates the applicability of traditional tracers when attempting to trace NAPL movement, and requires the identification of a new tracer.

Alginate hydrogels are non-toxic biodegradable material that can be impregnated with different materials (George and Abraham 2007). They are developed from plant proteins (George and Abraham 2007). Commonly used in drug delivery, they are non-toxic when released in the environment. Hydrogels can be constructed with different properties, allowing their density and other properties to be modified to match NAPLs. Hydrogels used in this project come from the National Energy and Technology Labs (NETL) Morgantown. Future work will address the ability of hydrogel to mimic the physicochemical properties of various NAPLs.

Flow Cell

3-D Printing

3-D printing or additive manufacturing is a technique to convert a computer-designed file into a physical object. Since creating a 3-D printed object only requires a

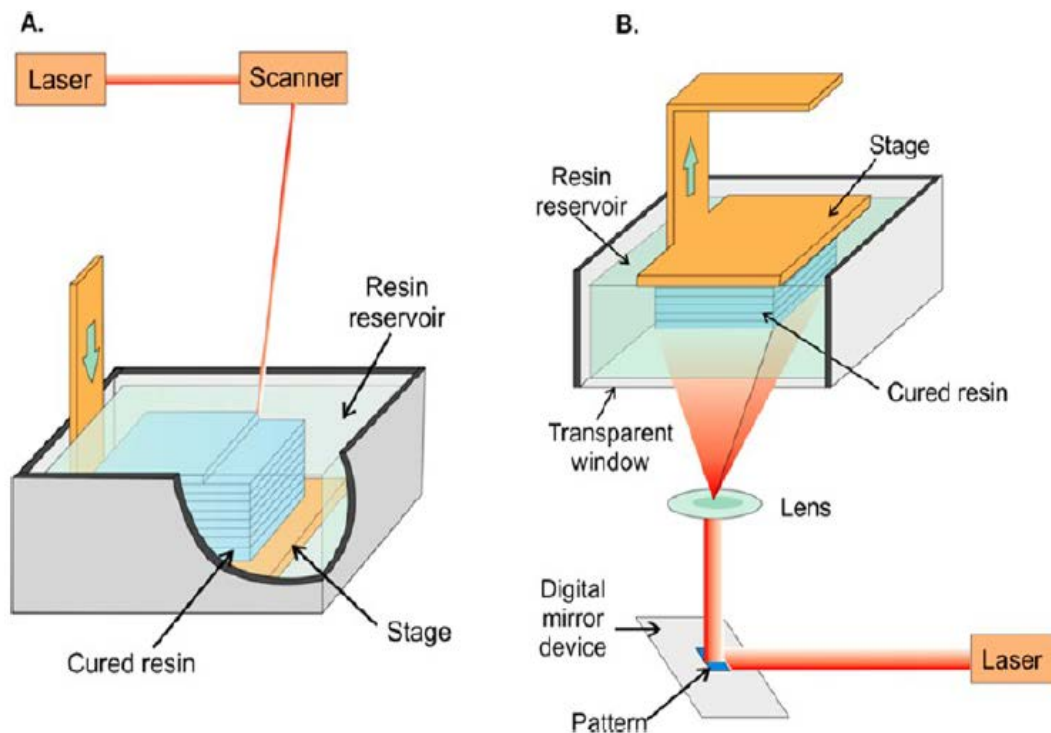


Figure 8 – Two diagrams of SLA process using light sensitive resin. A) The stage is leveled just below the surface of the liquid resin bath. A single laser beam is directed and traces out the shape of one layer of the object, hardening that resin. The stage sinks beneath the surface of the liquid in preparation for the next layer's creation. B) The stage is submerged in liquid resin a defined distance and a laser traces a layer, hardening the resin between the transparent window and the stage. The stage raises incrementally then dips back into the liquid resin to prepare for the next layer (Gross et al. 2014).

digital design file, a printer, and material, identical objects can be easily reproduced.

Iterating design allows for precise geometries to be produced and their impact on the flow system to be easily assessed. This creates a controlled testing environment as well as the ability to conduct destructive tests on a printed sample without fear of ruining the sample as the flow cell can be easily reconstructed from the digital file.

There are three common techniques to transform digital files into physical objects, stereolithography (SLA) (Figure 8), fused filament fabrication (FFF) (Figure 9), and selective laser sintering (SLS) (Figure 10). One of the key outcomes of this project is

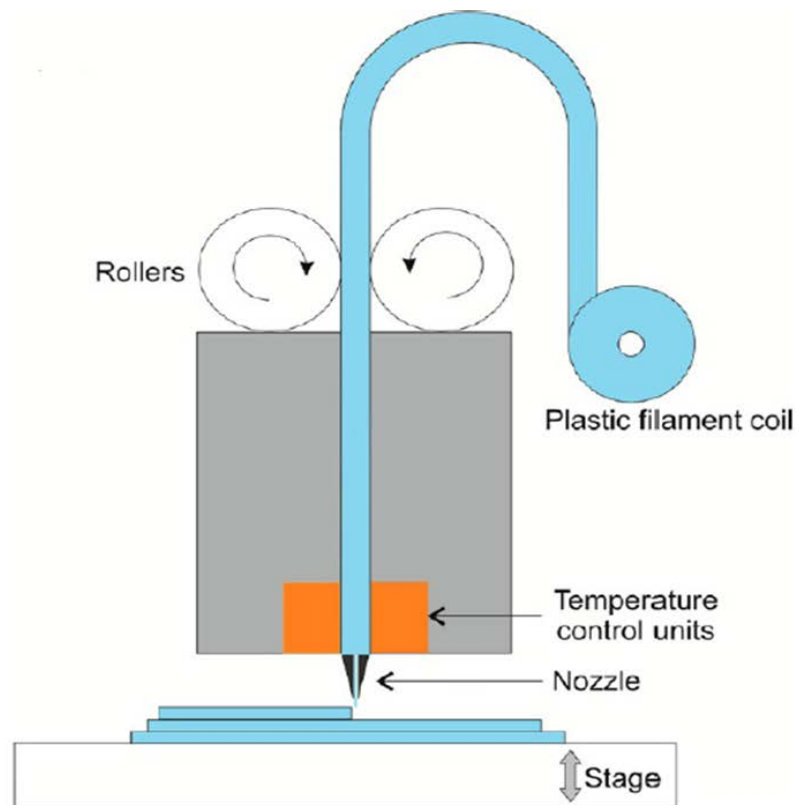


Figure 9 – Diagram of fused filament fabrication (FFF). Plastic filament is fed from the spool and heated in the nozzle to a specified temperature. The hot plastic is extruded out of the nozzle and deposited layer on layer according to an uploaded computer designed file (Gross et al. 2014).

determining which method is most applicable to function at the conduit scale.

Fundamentally, all additive manufacturing techniques construct objects by laying down successive layers of material according to computer-determined plans. They differ in the materials that can be used and their joining methods. SLA uses a photopolymer that hardens when exposed to ultraviolet light; FFF uses heated plastic filament that is then cooled; and SLS uses heat to sinter or glue to attach powdered metal, sand, gypsum, or other granular material together.

A digital design file is sliced horizontally to provide plans for each layer. Layers are laid down successively on a flat construction surface, known as a bed, which changes height incrementally to provide space for the next layer. For all additive manufacturing processes thin structures and walls are more complex to print and require support during printing to prevent deformation.

FFF is the cheapest and most widely available additive manufacturing process. This thesis utilized this FFF to construct flow cells, so some important design parameters will be discussed. Further reading and a general overview of SLA and SLS printing can be found in Gross et al. (2014).

FFF extrudes plastic filament through a heated nozzle and deposits the filament onto a flat construction surface. The previous layer begins to cool before the next is deposited. FFF prints can have variable infill values, the percentage of interior empty space that is filled with plastic. A print with 0% infill will only consist of shells, or outer layers, and has little structural strength. A print with high infill values does not cool quickly enough between layers to harden, so it tends to slump and deform under the

overlying weight. This issue is not present in SLA or SLS as there is no need to cool between layers.

Critically, in FFF printing with plastic, the joins between plastic filament layers are not precise, resulting in permeability. This could be due to uneven heating across the filament, uneven cooling on the print itself, plastic contraction during cooling, or another mechanism. SLA prints are impermeable; however any blockage in the laser, or uneven distribution of pigment in the resin can result in asperities or failed prints. FFF and SLA are standard 3-D printing techniques that see a wide range of applications inside and outside of academia. SLS requires a controlled environment and is prohibitively

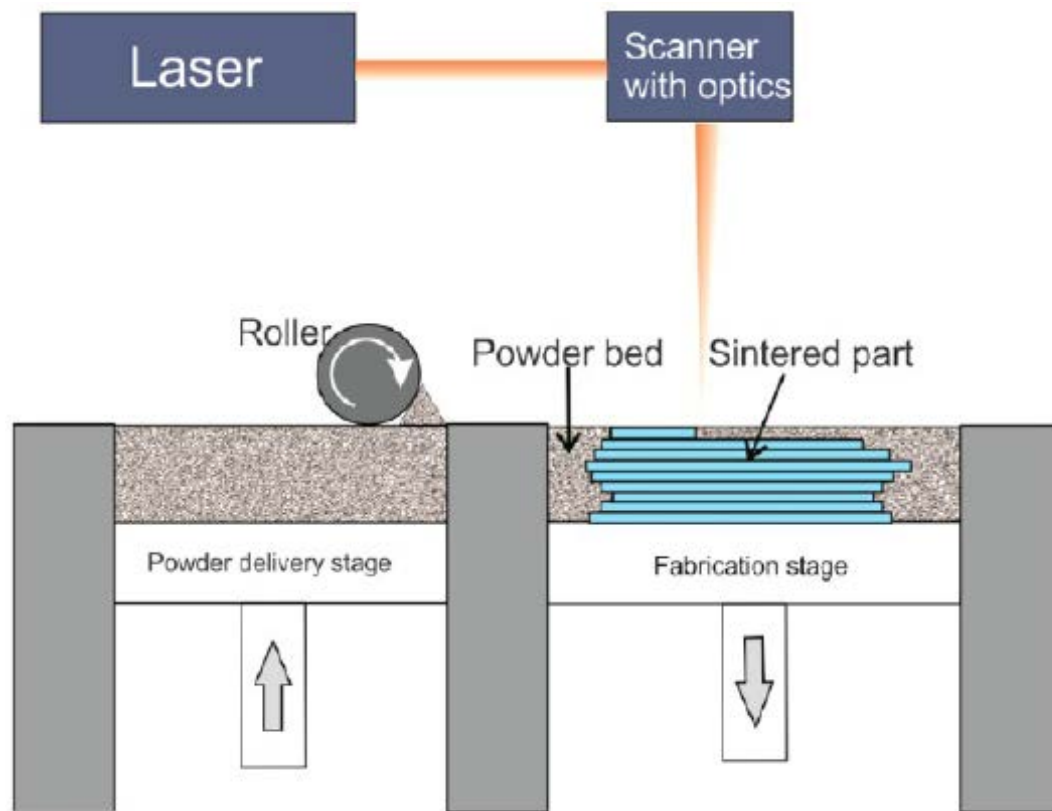


Figure 10 – Diagram of SLS printer. A roller pushes powder onto the stage. A laser sinters the powder together in the layer pattern. The fabrication stage lowers a determined amount as the powder stage raises a determined amount. The roller pushes another layer of powder onto the fabrication stage, and the process is repeated (Gross et al. 2014).

expensive. FFF is significantly less expensive than SLA, and allows for different materials to be used.

The highly customizable nature of 3-D printing makes it a compelling tool to use to explore difficult issues. At the macro scale ($>1\text{mm}$), the limitations of 3-D applications are the limitations of computer design. Unlike conventional manufacturing, 3-D printing can quickly create precise models and flow cells. These cells are easily reproducible, and reconstructed. Rapid development also allows for an iterative design process to accurately model problems. SLA in particular has been applied exploring vuggy Floridian karst water flow (Floreas 2009), water and air burst interaction in porous and fractured media (Crandall 2007), and fluid transport through designed porous media (Maggi 2015).

Imaging

X-ray computed tomography (XRCT) is the technique used in this project to image fluid inside the opaque conduit. Wildenschild et al. (2002) describe the XRCT process as a concentrated beam of x-rays directed towards the sample that are differentially absorbed and reflected depending on the sample material. The reemitted energy is detected and an image is formed (Figure 11). If the sample is held in a constant position and the incident beam is rotated around the sample, a 3-D image can be constructed. Successive images can be taken and have been used to characterize fluid infiltration in porous media (Singh et al. 2011, Dann et al. 2010). A useful set of images, one that can be used to validate the use of hydrogel beds as behaving the same way as NAPL, must have enough contrast between different experimental components and be taken quickly enough to capture flow.

XRCT is a non-destructive imaging technique that can characterize internal structures of a rock core (Baraka Lokmane 2009). For example, XRCT has been used to predict contaminant diffusion (Polak et al. 2003), characterize two phase flow along a fracture (Alajmi and Grader 2009), understand fracture apertures (Keller 1998), and create 3-D representations of complex pore networks (Brunke et al. 2007). For further

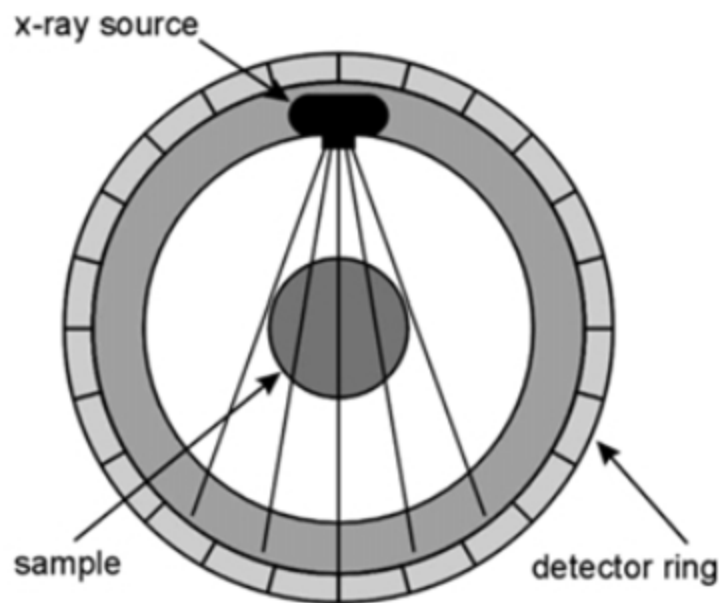


Figure 11 – Diagram of XRCT process. Measurements are made quickly enough to generate time stepped footage to understand flow in conduit (after Wildenschild et al. 2002).

examples of XRCT applications readers are directed to Cnudde and Boone’s review of non-destructive imaging applications (2013).

Methods

The project unfolds in two stages. The first is the construction of a conduit. Construction begins with a digital creation of the conduit, followed by FFF printing. The second is imaging NAPL-water flow through the conduit using the XRCT scanner.

Digital design

Computer Aided Design (CAD) is a type of computer program that can be used to digitally engineer precise 3-D objects. CAD software allows the creation and manipulation of two and three-dimensional objects in digital space. CAD software is precise in allowing the designer to specify the dimensions of all object characteristics. The program used is Solidworks, one of many CAD software packages, that was selected for its availability and ease of integration with local 3-D printers.

This software is robust and enables the design of a variety of conduits. This project begins with the simplest case to optimize the workflow and work through design, construction, and imaging issues. The first conduit designed is a meandering tube with elliptical cross section. This overall geometry is congruent with Palmer's classification (1991) of phreatic caves created by meteoric water (Figure 2). At this stage in the project the angle of meander and sinuosity are not specific as the aperture is the main controlling characteristic in promoting turbulent flow. This project is not intended to perfectly simulate a natural cave system. Instead it is to represent conditions likely to arise in phreatic conduits to show that our tracers are viable to use in the field. The ellipses in all of the conduits created for this project are at least 1 cm cross sectional area because a 1 cm conduit aperture has been identified as promoting the transition to turbulent flow (White 2002).

The conduit is constructed using a variety of different operations in the Solidworks program. To create an object in Solidworks first, it must be defined on a two-dimensional plane and then extruded in the third dimension. Solidworks allows the user to sketch a

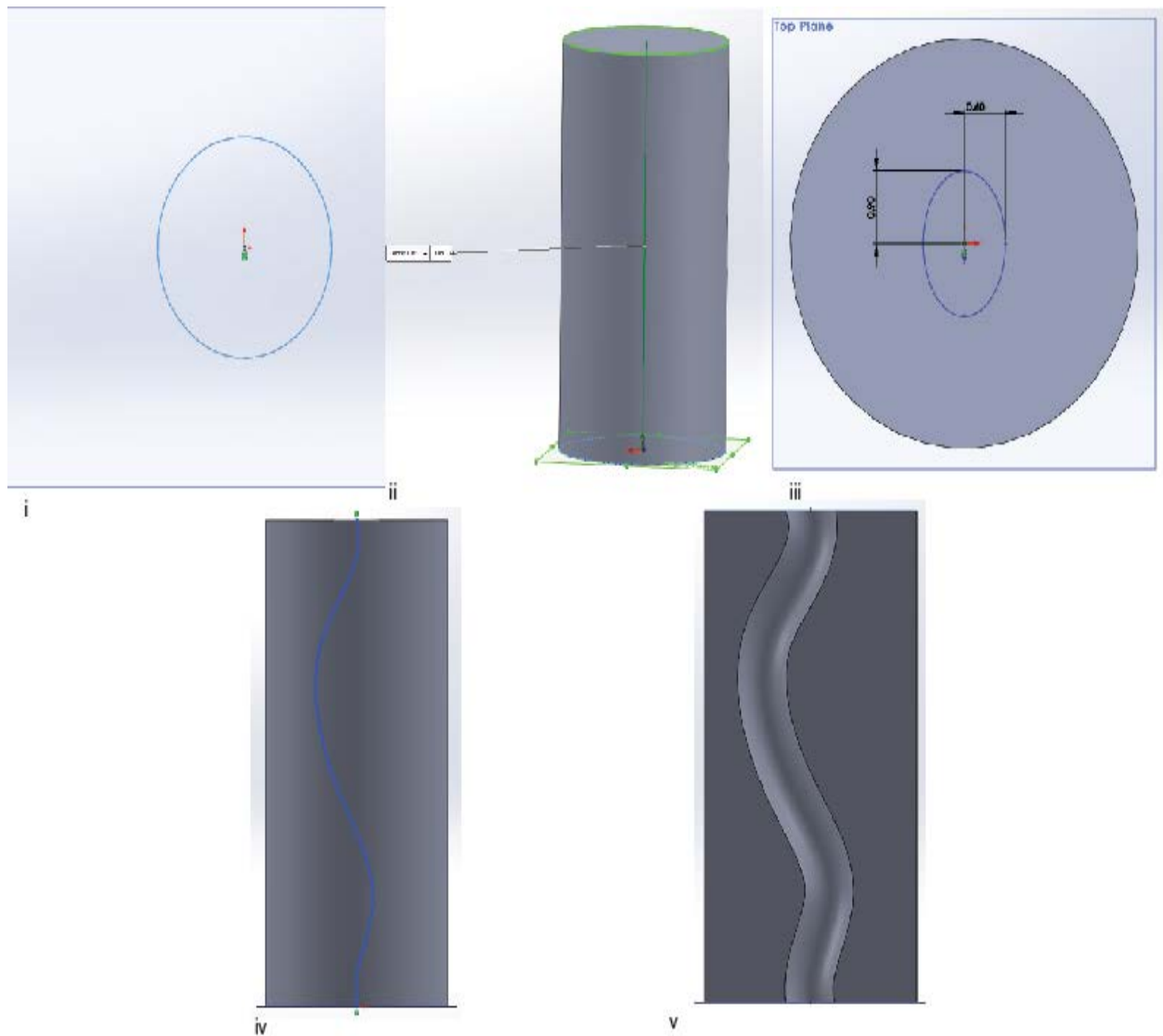


Figure 12 - Sequential images from Solidwork showing the construction of the cylinder and conduit. A circle is drawn on a plane (i), then a cylinder is extruded into the third dimension from that circle (ii). To create the conduit, an ellipse is sketched on the surface of the cylinder (iii), the path of the conduit is defined by the blue line intersecting the ellipse (iv). Finally, the cut sweep function is performed creating the conduit (pictured light gray) by removing the ellipse profile along the defined path (v).

variety of shapes including circles, quadrilaterals, ellipses, lines, arcs, and curves.

Sketching a square in two dimensions and then extruding the square into the third

dimension creates a cube. Drawing a circle and extruding it into the third dimension to the desired length creates a cylinder (Figure 12).

Digitally, all conduits are cut out of a 10 cm cylindrical core. On the computer all of the dimensions are defined precisely so when the object is printed, it will be compatible with the Hessler-style core holder. At NETL in Morgantown WV, collaborators have adapted a medical CT scanner with a Hessler-style core holder to image the printed cores. The Hessler-style core holder is compatible with standard rock core dimensions, 2.54 cm, 3.81 cm, and 5.08 cm diameter cores that are up to 2m long. Our imaged core and future cores are 2 m long to allow maximum flow length to image flow dynamics. Because the CT scanner requires a certain amount of time to create a single image, longer path lengths increase the likelihood of capturing contaminant flow through the core. To allow maximum space for sinuosity, core diameter is set as 5.08 cm.

On a digital shape flat face two-dimensional shapes can be drawn and new extrusions or cuts can be made. Cuts are negative extrusions. To create a conduit, an ellipse is drawn on one face of the cylinder. An ellipse is drawn by selecting the plane to sketch on, selecting the ellipse tool, clicking to set the center point, then defining the major and minor axes. The ellipse can be constructed anywhere on the face, but keeping each start and endpoint in the center of the cylinder face eases the construction of the entire conduit. Centering the ellipse is simplified with automatic snap-to tools in Solidworks.

Using the sweep cut tool, the ellipse on the cylinder face can be cut out of the cylinder creating the analog phreatic conduit. A sweep cut cuts a selected shape or profile along a defined path. A sweep cut can only be executed if a closed polygon is selected as a profile, the path intersects with the profile, and if the final cut does not cut its own path. To achieve this, the object is oriented upright in digital space. Solidworks enables the user to sketch on a series of predefined planes. Begin by sketching a line on the predefined front plane; the line should automatically be drawn through the center of the cylinder. The path should be curved, but the path should have enough of a buffer on either side so that when the profile is cut, it will not pass through the path. In this first case, if the major axis of the ellipse is 1 cm, then the path needs .5 cm space on either side to cut. The conduit should not exit the side of the cylinder, nor pass within 5mm of

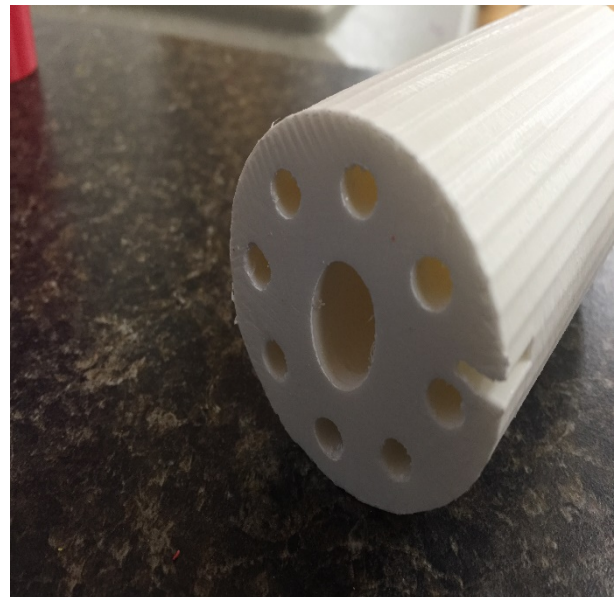


Figure 13 – Photograph of post-hole connection system

the edge to promote structural stability in the printed object. To add complexity to the conduit such as traps, obstructions, or branches another plane must be created to sketch a new profile. The same processes of defining a profile and path to execute a sweep cut can be used to add complexity to the conduit. Profiles and paths must be sketched on planes perpendicular to each other.

Connecting a series of core segments is vital to successful imaging. The XRCT imaging relies on water tight, seamless connection between segments. Prints are constructed with a post-hole system to connect successive core segments together (Figure 13). Circles are sketched on the faces of each cylinder. The sketches are repeated in an equally spaced circle around the perimeter of the cylinder. One set of circles is extruded to create the posts, while the other is cut slightly longer to create holes. The holes should be at least 1 mm larger radius than the posts to enable epoxy to adhere the posts to the edges of the holes.

Designing a simple digital meandering conduit, once the user is familiar with the program takes about 1 hour. Increasing complexity increases the time needed to design as transformations and digital planes must be inserted and manipulated. Scaling a map into digital space, the most complex design action, can take upwards of 8 hours even with mastery of the program.

Printing Technique Overview

Both SLA and FFF were evaluated as potential construction methods for this project. SLS was not evaluated for this project because it is not available on campus. Printing core segments using SLA and FFF yield similar results. To determine which method to

use for this project, a series of test prints were conducted using both SLA and FFF. The main difference between the printing methods is the permeability of FFF prints. SLA creates solid walled, impermeable prints, in contrast to the FFF prints that are permeable. SLA resin is significantly more expensive than FFF materials. While both printing techniques require temporary automatically generated support to be created to hold open void spaces, the threshold for necessary SLA support is lower. This translates to more support needed in SLA prints when compared to FFF objects. SLA support is typically more difficult to remove and removing it can cause structural damage.

Acetone Treatment

Permeability in 3-D prints presents a problem for XRCT imaging. This project aims to focus imaging strictly on conduit flow. If the print is permeable, fluid from the conduit can seep and stain matrix outside of the conduit. If there is communication between the conduit and the surrounding matrix, not only will results be impacted, but also each run could leave a residue that might interfere with future runs on the same core. ABS plastic contains acetophenone, which is soluble when exposed to acetone (Lide and Milne 1994). Exposing ABS prints to acetone vapor is a common technique for forming a smooth surface used by hobbyists (zkus 2016). When exposed to acetone the plastic melts into a liquid. The liquid flows, and then hardens once the acetone evaporates. To make FFF prints impermeable, and therefore eliminate potential contamination from the conduit to the matrix, the hobbyist technique is adapted.

ABS cups were exposed to 20 min, 25 min, 30 min, 35 min, 40 min, and 45 min at room temperature. The 40 and 45 min exposed cups saw significant structural deformation; the vapor had weakened critical points of the structure. The 25 and 30 min

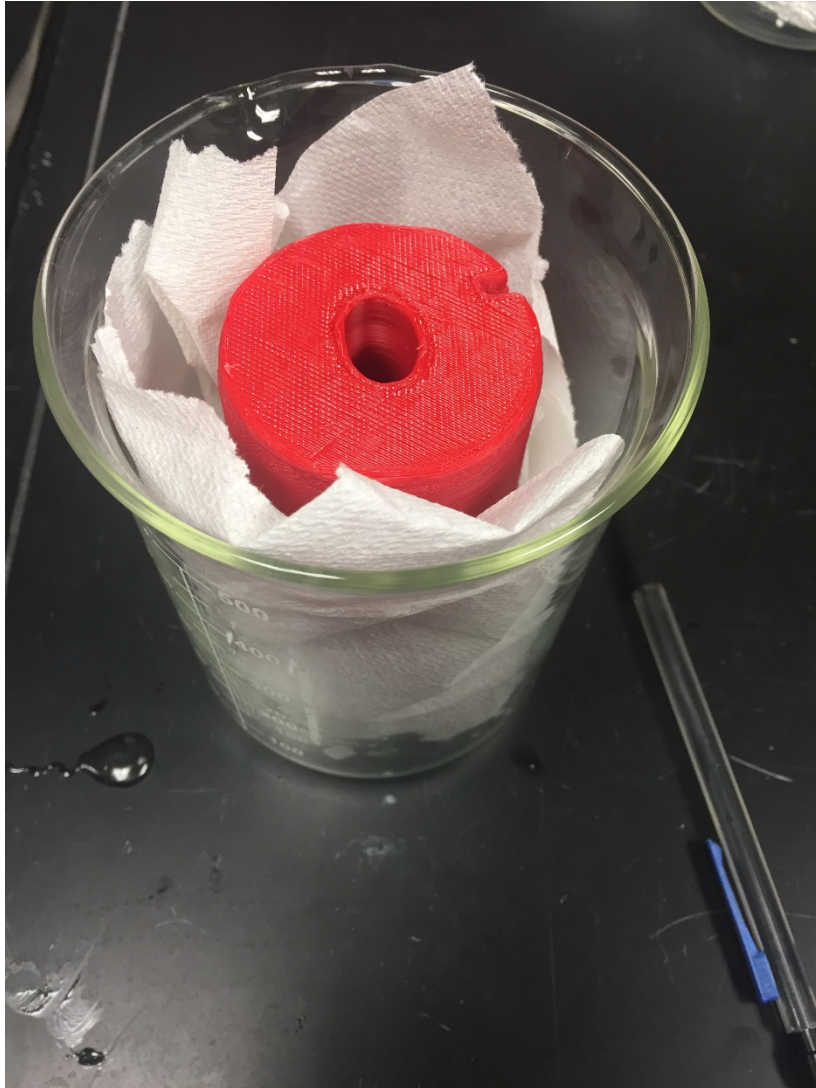


Figure 14– Photo of acetone treatment chamber. A glass beaker is lined with paper towels with the conduit segment in the middle. Paper towels are soaked in acetone; beaker is covered; and acetone evaporates and dissolves the surface layer of the core segment. Paper towels cannot touch the conduit itself else the acetone will cause the structural integrity of the conduit segment to deteriorate. As such, the entire core is mounted on a piece of aluminum foil.

exposed cups did not exhibit significant impact from the exposure to acetone. The outside of the 35 min cup was smoothed, so this treatment time was selected as having significant acetone influence, while maintaining structural integrity.

The print that is being treated is placed on an aluminum foil tray in a glass beaker lined with acetone soaked paper towels (Figure 14). Direct contact with acetone will destroy the segment. Keeping the segment suspended on a platform protects the segment while also allowing vapor to flow into the conduit itself. Soaking paper towels in acetone allows for a constant release of acetone vapor into the beaker.

Permeability Assessment

Printing techniques and materials were evaluated for their ability to create a leak free water container. Small scale tests were conducted before time, material, and energy were invested to create the series of core segments.

Four cups were printed out of clear resin, acrylonitrile butadiene styrene (ABS), acetone treated acrylonitrile butadiene styrene (a-ABS), and polylactic acid (PLA). The resin cup was constructed using the SLA printing technique; the others, ABS, a-ABS, and PLA cups, were printed using FFF technique. Each cup is 2 cm in diameter and 5 cm tall (Figure 15). A simple experiment was conducted to assess printing concerns by filling each cup with water and monitoring the water level for 15 hours. The SLA cup drained immediately, due to a small hole in the base of the cup. This was most likely a result of printer error. Errors like this can occur because resin is prematurely exposed to outside light causing solidifying outside of intended pattern. They can also occur because the laser tracing the layer outlines is not properly focused. Instead of conducting multiple

prints to test the incidence of printer error, SLA was discarded as an option outright due to its high cost, tendency to produce errors in print, and requirement for supports that make generating smooth conduits difficult.

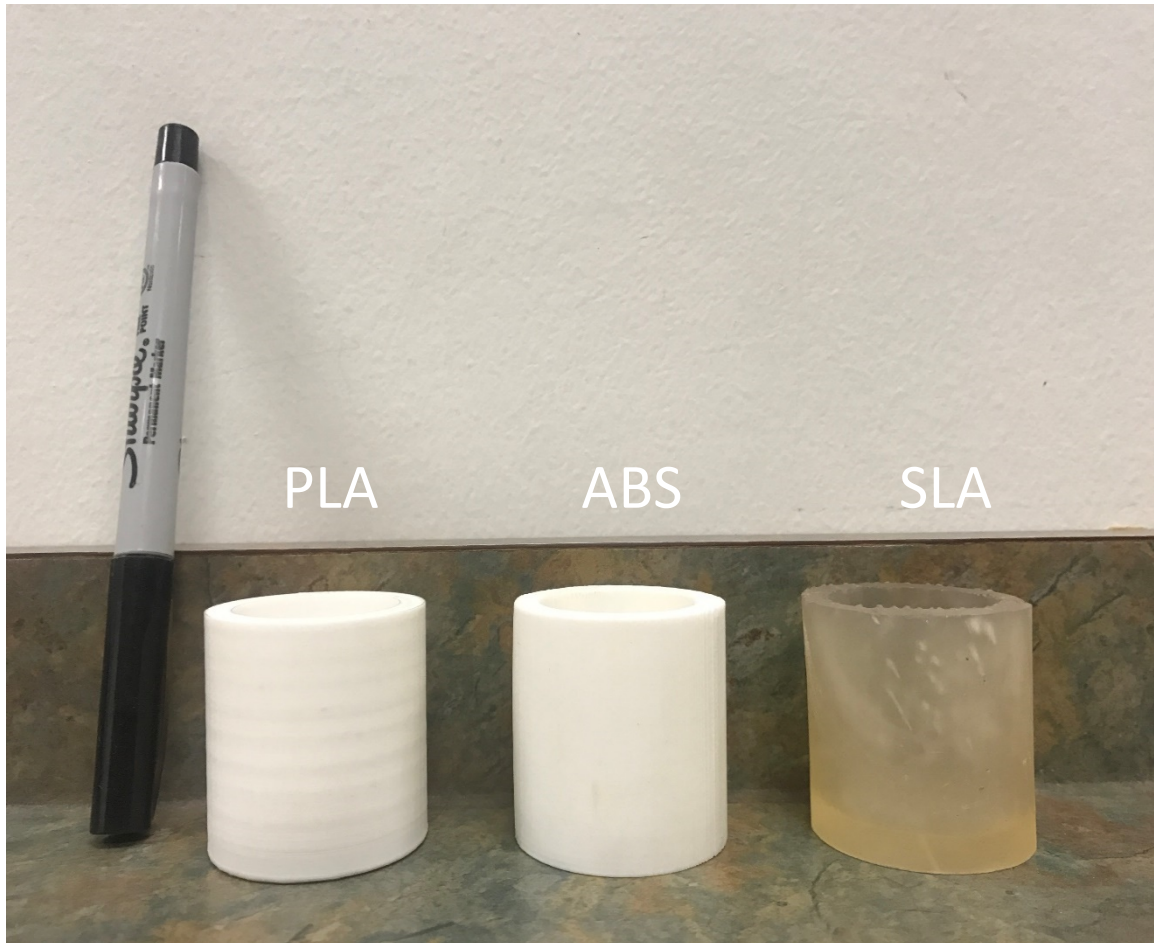


Figure 15 – Photo of printed test cups before they are filled with water. The lighter spots on the SLA cup are remains of automatically generated support that could not be smoothed. Aside from printing defects in the cup, those nubs make controlling conduit wall roughness difficult. Not pictured is the impermeable a-ABS cup.

Both the PLA and ABS cups had water leaking through the base after 15 hours. Both cups were printed with the same printing characteristics including filament size, layer spacing, and infill percentages. The a-ABS cup that was treated by exposing to acetone,

an adapted hobbyist technique, did not leak for the entire 15 hour period. Because the acetone treated cup was able to hold water for extended period of time, this FFF treatment method was selected for making impermeable core segments.

FFF of Conduits

After the digital object has been designed, it must be converted into a file format that specifies for the printer where and how to deposit the filament. The completed conduit segment to be printed is saved as a .stl file. This file format can be converted by a variety of programs into a .gcode file. Gcode is a common file format used by printers to slice the digital file into layers that can be printed. Simplify3D, the program used in this project enables the user to identify extrusion rates, extrusion temperature, inclusion of support, infill percentages, bed temperature, raft criteria, and other printing options (Table 1). After several trial runs these settings proved the most reliable for creating precise accurate prints using ABS plastic.

The most important non-standard settings for this project are infill percentage, bed temperature, extruder temperature, print quality, inclusion/exclusion of support, and inclusion/exclusion of a raft. Infill percentage is set at 20% to provide some structural support while optimizing print speed. Infill pattern can be rectangular or triangular; the stresses on the final product are not significant enough for that setting to have a large impact. This project uses rectangular infill pattern. The makerspace where the segments were printed have a series of cubes that demonstrate different infill percentages. Cubes that are printed with 0% infill are exceptionally weak and deform with little pressure. Recommended infill percentages are between 20 and 40% to optimize amount of filament

needed while providing support to the print. Infill percentages greater than 80% tend to deform because the plastic is unable to cool and set in the desired pattern. That level of infill also uses significantly more filament. The 20% infill settings are selected without testing, based on technician recommendations.

Using ABS filament necessitates an extruder temperature of at least 112.7° C (235° F) to melt the plastic. If the temperature is set higher than 118.3° C (245° F), the plastic is too hot and will likely not deposit properly. The bed temperature is set at 43.3° C (110° F) Fahrenheit so the extruded plastic will adhere to the bed. Because the FFF is inherently permeable and the prints will be treated with acetone to seal the conduit from the matrix, print quality is not critical. Print quality involves a tradeoff between layer height and speed of print, and for this project medium quality is adequate. Longer prints have more opportunity to make print-ruining mistakes, and medium quality is sufficient.

A raft is a flat base that can be added onto any print to increase adhesion as ABS adheres better to ABS than the glass bed. The raft is removed at the end of the print. Because most of the prints here have flat bottoms, a raft is not critical. Simplify3D can automatically generate support that can be removed at the end of the print. Support allows parts of the print to cool and harden in the proper shape when it might otherwise sag and deform. However for the size of empty spaces in the conduit segments, support was not needed. ABS plastic is strong enough not to deform under the design conditions.

Conduits are printed on a Makergear M2 printer. The maximum build volume of this printer is 20.3 cm x 25.4 cm x 20.3 cm (Makergear 2017). The XY dimensions of the conduit fit inside this build area, but the entire 2 m core cannot be printed in one

complete section. Printing tall objects requires more time and increases the possibility of a mistake due to decreased stability and increased weight. As additive manufacturing is a successive process, one mistake can ruin an entire print. To mitigate this risk and to print a core segment in a single workday, core segment height is set at 10 cm tall, and 20 pieces are joined together to create the final 2 m core for imaging.

Construction

After the each core segment has been treated with acetone vapor, the core segments must be connected to form the full 2 m extent (Figure 16).



Figure 16 - Photograph of completed core and with attached 1/8" inflow tube. Green areas are core. Everything has been wrapped in Teflon and plastic to seal the conduit (Moore 2016).

GORILLA epoxy is placed on the end of each post and spread around the base to glue each segment together.

To flow fluid through the system, it must be watertight. Epoxying the core-segments together does not create a sufficient seal throughout the conduit. The entire system is covered in Teflon and plastic wrap. One port is installed at each end to provide an inflow and an outflow (Figure 17).



Figure 17 – Photograph of constructed core ends with inflow and outflow tubes attached.

Flow Components

Inside the conduit is a two phase water-NAPL system or water-NAPL analog system. This overall project eventually will identify the correct formulation of alginate hydrogel beads to mimic NAPLs. Beads for this first experiment we are created at NETL Morgantown and are denser than water, but haven't yet been validated as NAPL proxies.

XRCT imaging differentiates materials based on atomic number. To provide enough contrast between hydrogel beads and water in the final image, beads should be doped with high atomic number materials like iodine. Beads in this initial experimental run are not doped with iodine. Water is pumped through the conduit through a single inflow and outflow tube under surface pressures and ambient temperature.

Imaging

X-Ray Computed Tomography (XRCT) is a non-destructive imaging technique that uses X-rays and their interaction with different materials to construct an image. The

HCH Series — Biaxial Type Core Holders

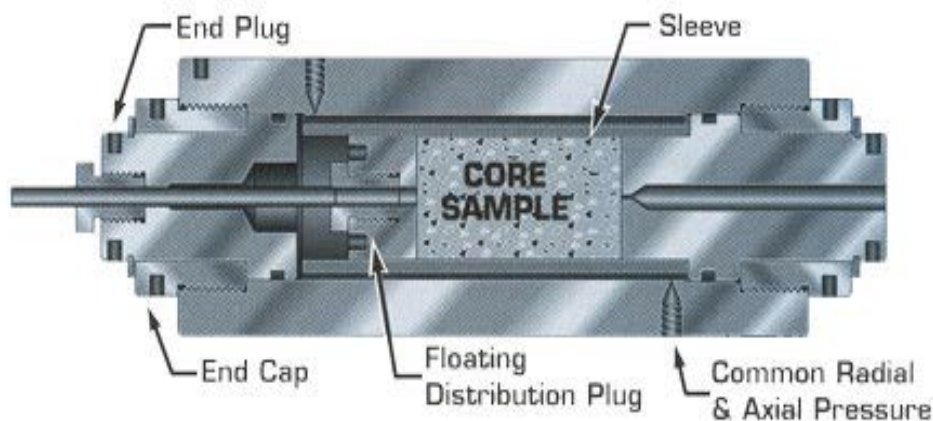


Figure 18 – Diagram of the Hessler-style core holder present in the XRCT scanner at NETL Morgantown (Core Laboratories 2016).

XRCT scanner used is a Toshiba Aquilion with a resolution of 250 micron X 250

microns X 1000 microns (NETL 2013). The scanner is outfitted with a Hessler style core holder to hold the sample in a constant position (Figure 18). A Hessler core holder is designed to apply constant pressure around a rock core. Though this project is flowing liquid at surficial pressures, NETL has installed these devices on the XRCT device, thus the printed cores are shaped like conventional rock cores.



Figure 19 - Cartoon of XRCT scanner. Sample is black cylinder in the middle of the detector donut. The flow control apparatus is outside the donut-shaped detector (NETL).

XRCT in this project is relatively macro-scale to lower the time needed for every scan to capture flow in the conduit. Data is collected by an x-ray source and detector rotating around a stationary sample (Cnudde and Boone 2013) (Figure 19). A beam of X-rays passing through a homogeneous material causes the object to emit secondary X-rays and electrons that can be used to determine material characteristics (Wildenschild et al. 2002).

Those secondary X-rays and electrons are detected and a linear attenuation coefficient can be calculated for a point based on the absorbed and emitted energy. Linear attenuation coefficient is a function of photon energy of the X-ray beam, electron density of the material, and effective atomic number of the material. Attenuation intensity is described by Lambert-Beer's law and is a function of sample thickness, initial beam intensity, and linear attenuation coefficient (Wildenschild et al. 2002). At energies less than 100keV effective atomic number controls linear attenuation coefficient. At higher energies, electron density has the most impact (Wildenschild et al. 2002).

Directing X-rays from one incident angle creates a two dimensional scan of the sample. By rotating the incidence beam and detector around the sample, multiple angles

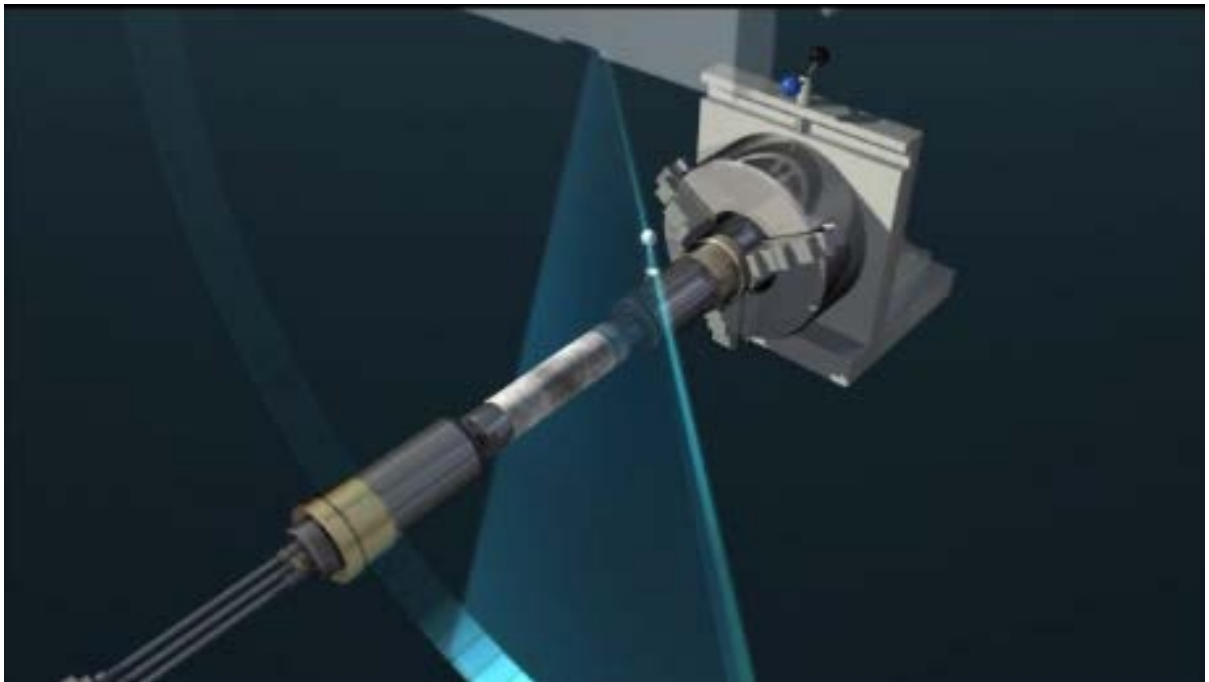


Figure 20 – Cartoon of X-Ray beam rotating around the sample. Detector ring is the pale blue ring. Gray cylinder is sample. X-rays are blue fan (NETL).

of data can be collected and algorithmically converted from a series of two-dimensional images into a 3-dimensional image (Cnudde and Boone 2013)(Figure 20).

The Toshiba Aquilion scanner at NETL has an energy less than 100kW. It has a 0.43x0.43x0.5 mm resolution, a 60 second scan time, and a 3 minute scan interval (Toshiba Medical Corporation 2015).

Flow Test

The assembled core is placed in a Hessler style core holder with a 1/8" inflow tube attached to one end and a 1/8" inch tube outflow tube. Water and hydrogel beads flow into the system as XRCT scans are conducted. Hydrogel beads were used during this test because they are significantly easier to handle than NAPL. The core is stationary as the incident beam rotates around the sample collecting plan and cross sectional images. In between scans the sample is moved slowly through the detector ring so the entire plan view of the core can be imaged. Images are collected and processed at NETL.

Results and Discussion

Flow System

A 1.5 m conduit was successfully constructed from a computer-designed file. Fifteen 10 cm segments were epoxied together using the post-hole system. The epoxy and acetone treatment were not adequate sealants to keep liquid isolated in the completed conduit, and some epoxy invaded the matrix space. That invasion made it difficult to determine some bead positioning in the conduit because the atomic numbers of the main

constituents of epoxy, beads, and ABS plastic were not significantly different enough to differentiate among the three materials. The entire 1.5 m core was wrapped in Teflon and then shrink-wrapped in plastic to stop fluids from leaving the system through core segment intersections (Figure 21). Epoxying the core segments together did not create a water tight connection, and therefore water was not able to flow through the system.

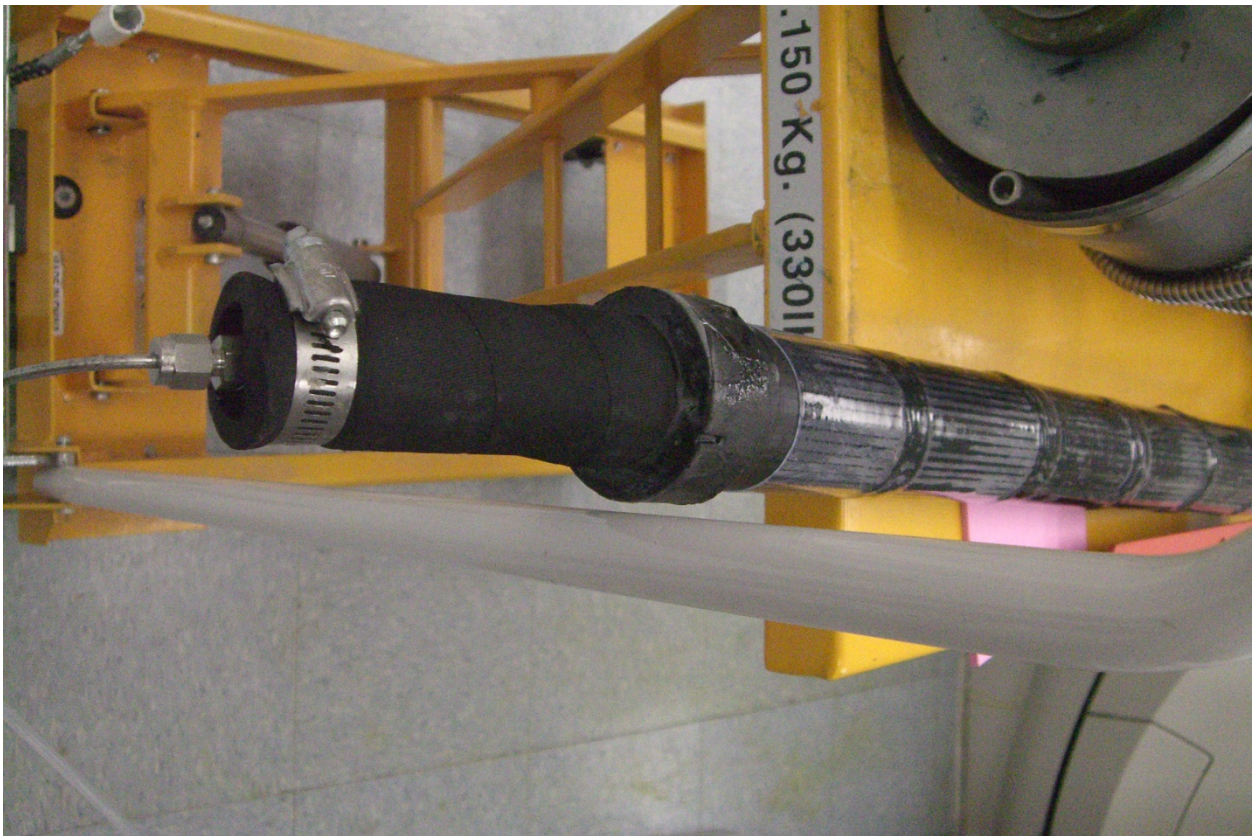


Figure 21 – Image of completed core before testing (Moore 2016).

Wrapping in Teflon and plastic kept the pumped hydrogel beads and water in the core system.

Beads flowed into the core through the inflow tube, but in the outflow tube the beads clogged together preventing beads from leaving the system. As the beads could not pass through, pressure built in the system and the core eventually ruptured prohibiting any subsequent experiments using the same core. However, XRCT scans of the test were still collected and provide useful information.

XRCT Data

Three types of data were collected during the experiment. The first is a composite image of the conduit that creates a digital three-dimensional image of the core (Figure 22). The composite images of the core show the scans are successful at differentiating between water and surrounding plastic. Composite images like this can be used to compare the shape of the design file, the anticipated conduit geometry, and to determine if the conduit is properly sealed. The composite image shows some areas where the conduit is irregular indicating a defect in core construction. This data is useful after a successful test to prove the conduit is accurately printed. Creating these three dimensional composite images do not provide information about flow in real time; however it can show if and how beads or NAPLs might pool in a system or leave the conduit. It can also show the location of residual contaminants if there is enough contrast between phases. All of the beads are flushed through the system and are not represented on the composite figure.

The second data type collected is a time-varying series of cross sectional two-dimensional images that should enable characterization of NAPL and water through the

system (Figure 23). The cross sectional view of flow shows beads in the conduit itself (Figure 23).

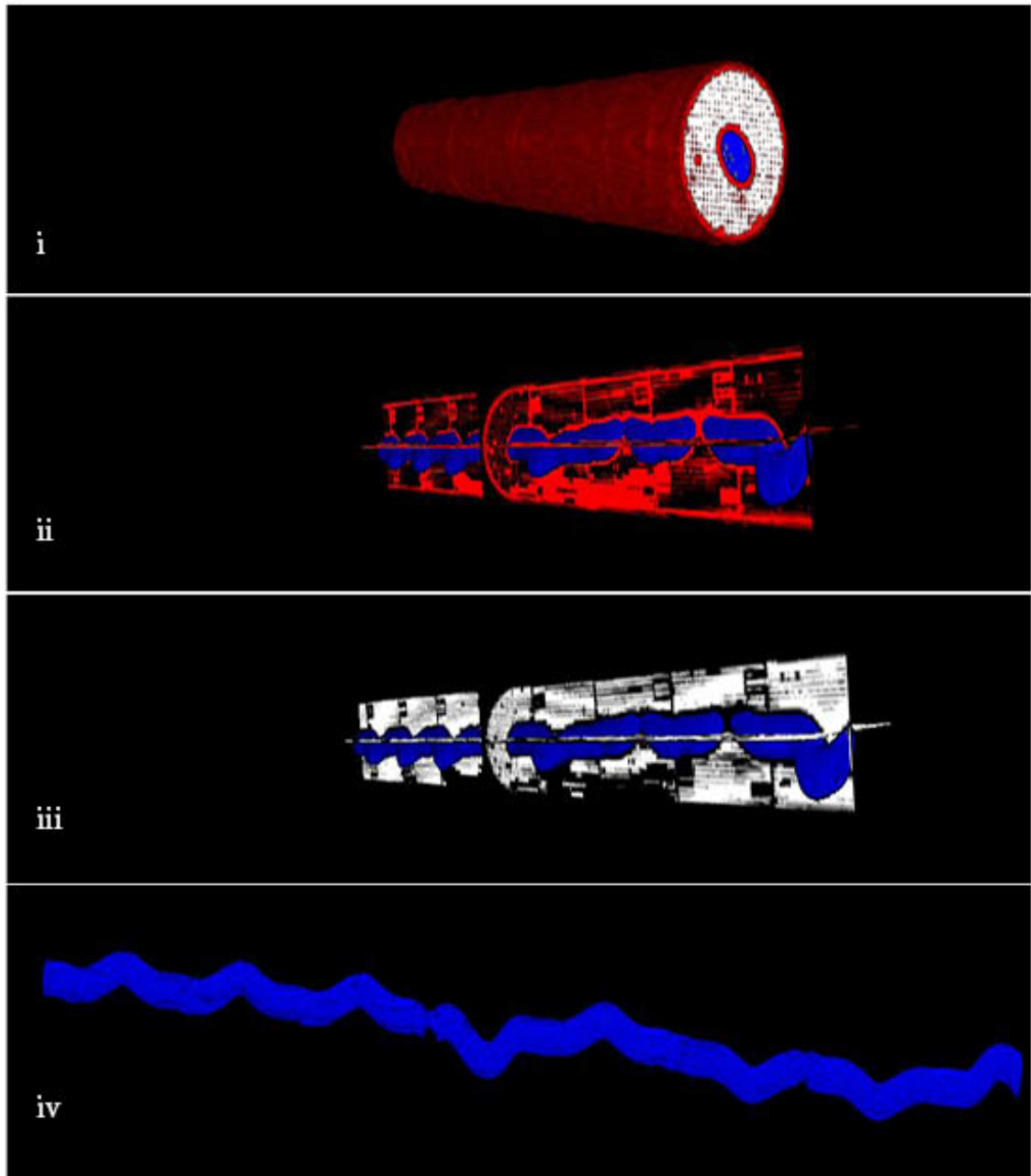


Figure 22 - Colored XRCT images combined to create 3-D digital reconstruction of core. Red is outer plastic, white is rectilinear structural plastic matrix, and blue is the conduit. Images i-iv strip each type of plastic down to the conduit. Notice the curvilinear geometry of the conduit in iv. Comparing the imaged conduit to designed conduit can help identify conduit ruptures and unwanted areas of conduit-matrix communication. This imaging strategy does not allow assessment of flow.

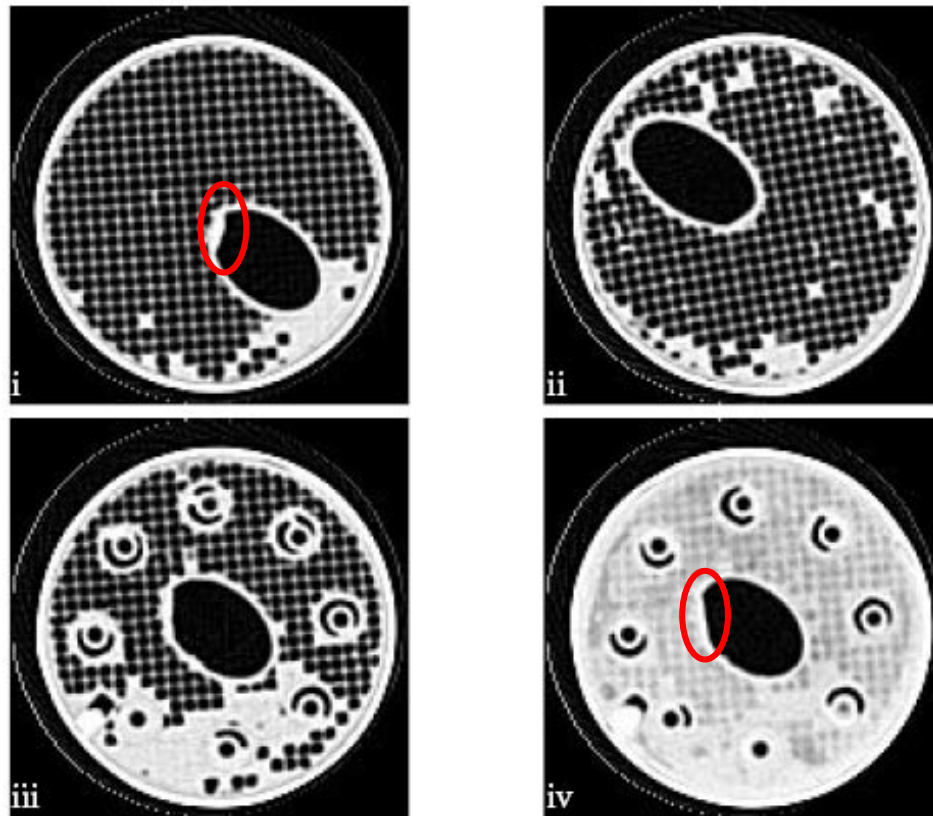


Figure 23 - XRCT images of ABS cores looking through the conduit. White grid in images i and ii are interior plastic supports and epoxy that has invaded the matrix. The black ellipse is the conduit. Note that the conduit is not in a constant position in relation to the rest of the core. This demonstrates its meander. Images iii and iv are taken near core-segment junctions. The equally spaced round circles are the post-hole connection system. Solid white areas are epoxy used to connect core segments. In each of the images note that the conduit is designed to have a smooth elliptical shape. The presence of irregularities circled in red is inferred to be beads moving through the conduit. Higher contrast between beads and epoxy and plastic would better show this phenomena.

The third image is a plan view of the system that can be used, in conjunction with the composite image, to see conduit geometries and defects (Figure 24). The plan view of the core should allow characterization along the length of the conduit (Figure 24).



Top



Middle



Bottom

Figure 24- XRCT images of ABS cores. Hydrogel beads and water in a meandering conduit flow from left to right. Black is water; gray is plastic; and white is epoxy. Images are plan views of the core at the upper, middle, and bottom third. The entire core plan is represented in each third. The top image shows the connected series of cylinders with epoxy invading the matrix around core segment connections and notches used for alignment. The middle image shows the conduit meandering through the core and some beads circled in red. Note there is significant epoxy invasion toward the midpoint of the core especially near connection points. The bottom image shows the lower portion of the core with significant invasion of epoxy into the matrix.

Both of these time varying image types illustrate the need to dope beads differently. The beads are currently too similar in atomic number to the surrounding plastic to be distinct. Because beads do not image differently than surrounding plastic their presence can only be inferred. It is unclear if the scan time is fast enough to capture flow along the conduit. A complete scan takes several minutes depending on sample size. We would expect to see evidence of movement in the plan view images, but do not. Given this information, bead movement can be inferred by examining the irregularities at the conduit wall. If the digital design file and composite image indicate a regular ellipse, but a cross section image does not show a regular ellipse, the irregularity is assumed to be from the beads. All three types of images are necessary for characterizing the flow of NAPL analogs through the conduit.

Further research

One of the purposes of this project is to demonstrate the capability of using FFF technology to craft specific flow cells. Designing a conduit for a project requires expertise. Working with a program like Solidworks and with some of the printing specifications used in this project should allow a researcher to manufacture useful flow cells. Some specific questions to be explored with FFF flow cells are:

- matrix-conduit interaction where the inherent permeability of FFF is used to simulate the matrix around natural conduits
- proto-conduit flow to examine NAPLs and water movement in young karst systems
- trapped DNAPLS in conduits with uneven floor or reservoir areas

- Flow obstructions to simulate sediment piles or other trapping mechanisms.

This is an incomplete list of potential research areas strictly related to conduit design. The bulleted list refers to future questions that may be designed to answer, however there is still work that could be done to improve the methodology. The use of construction material could also be explored further. More rigorous analysis could be conducted with a series of cups and a series of timescales to determine the incidence of SLA printer error. Settings used in FFF printing could be changed. A shift to 'high' quality prints in conjunction with a shorter acetone exposure time may function to seal the conduit sufficiently.

Acetone treatment was used in this project to seal the conduit from the matrix. This process is not exact; thus it may be replaced in future work in favor of a liquid sealant. Using a liquid sealant along the edges of the conduit completed in the core may double as a segment sealant as well as conduit sealant. Qualitative experiments have shown epoxying flat surfaces is more effective than the post-hole system used in this project. The post-hole system is fragile and does not create a flush surface, and creates avenues for epoxy to invade the conduit, though it does align the core segments. These problems are avoided in a flat surface epoxy.

Overall core shape may be flexible. Instead of being restricted by traditional rock core dimensions, a different holding and imaging setup may be utilized to provide more room for conduit complexity. Rectangular prisms for example provide large flat faces to join segments and more space for the conduit to meander.

This project has not determined if two phase flow can be adequately imaged with the Toshiba Aquilion XRCT scanner. It is still possible that the scan time is too long to capture flow along the conduit. Beginning projects with liquid NAPL instead of beads will prevent blockages and subsequent catastrophic failure. It is unclear given the current information if liquid NAPL alone contrasts enough to be distinguished from plastic and/or epoxy. In future experiments NAPL or water should be doped with a high atomic number material like potassium iodide to provide contrast (Moore 2016).

Conclusion

The ease of translating a CAD file into a dimensionally defined conduit solidifies this technology as a valuable tool in karst studies. Overall, accurate flow cells were created that are reusable and can be modified to simulate different conditions easily, but the process needs further refinement to reach its full potential.

FFF is a printing method that quickly, reliably, and inexpensively was used to create customized flow cells. It is more accessible than SLS and more scalable than SLA. To address the inherent permeability of FFF, ABS core segments were exposed to acetone to seal the conduit from the matrix. Because only one experimental run was undertaken, it is unclear if the acetone treatment explored here fully sealed the conduit from the printed matrix porosity. Further experimentation has shown that coating the conduit walls with liquid rubber, epoxy, or some other material to seal the conduit is a reliable way to create a seal.

Imaging turbulent or other relatively high energy phenomena requires a minimum path length that cannot be achieved in a typical 3-D printer's build volume. To utilize this

imaging technique, effective methods of joining segments together must be identified.

The post-hole system is complex and does not provide an adequate seal in between core segments, though the posts ensure a continuous, aligned conduit. Instead flat surfaces that have some method of alignment would be more practical. A flat surface provides a better surface to adhere to and reduces the possibility of epoxy invasion into the matrix.

It is unclear if flow can be adequately imaged in this experimental configuration. There was only one successful imaging sequence. Hydrogel beads, the analog for NAPL, can be inferred in the conduit; however the contrast in the XRCT scan between bead, plastic, and epoxy is minimal. To ensure effective imaging, one element of the system should be doped or impregnated with high atomic number material. Maintaining a neutral effect on density is key to achieving an actual analog NAPL behavior.

Communicating information from the scans is best done through animated pictures. Side by side comparison of movies of different NAPLs or beads under the same conditions i.e. pressure, temperature is the best way to characterize flow using this information.

Printer: Makergear M2 Filament: Hatchbox ABS 1.75mm filament	
Nozzle Diameter	.35mm
Extrusion multiplier	1
Extrusion width	.4mm

Retraction Ooze Control	
Retraction Distance	1mm
Extra Restart Distance	0mm
Retraction vertical lift	0mm
Retraction speed	1800 mm/min
Coast at end	No
Wipe nozzle	No

Layer	
Layer Height	.2mm
Top solid layers	3
Bottom solid layers	3
Perimeter shells	3
Outline direction	Inside
First layer height	100%
First layer speed	50%
Optimize start point	Yes

Additions	
Use Raft	Yes
Extruder	Primary Extruder
Raft layers	3
Raft offset from part	2mm
Separation distance	.25mm
Percentage raft infill	40%
Diaphragm	No
Support	No
Skirt	No
Prime pillar	No
Ooze shield	No

Infill	
Infill extruder	Primary extruder
Internal fill pattern	Triangular
External fill pattern	Rectilinear
Interior fill percentage	20%
Outline overlap percentage	15%
Infill extrusion width percentage	100%
Minimum infill length	5mm
Sparse infill	Every layer

Temperature	
Heated Build Platform	110°F

Cooling	
Fan Speed	60%
Adjust printing speed for layers below	15 sec
Speed reductions down to	20%
Fan Overrides	No

G-Code	
5-D Firmware (E version included)	Yes
Relative extrusion distances	No
Allow Zeroing of extrusion distances	Yes
Independent extruder axes	No
M101/M102/M103 commands	No
Firmware supports sticky parameters	Yes
Apply total head offsets to G-Code coordinates	No
Cartesian robot	Yes
Build Volume	
X	200mm
Y	250mm
Z	200mm
Origin Offset	No
Toolhead Offset	No
Homing direction	Minimize distance
Flip build table axis	Y-axis
Firmware	Rep-rap
Baud Rate	115200 bits/sec

Other	
Printing speed	3600mm/min
Outline underspeed	50%
Solid infill underspeed	80%
Support structure underspeed	80%
XY axis movement speed	4800mm/min
Z axis movement speed	1002mm/min
Horizontal size compensation	No
Filament diameter	1.75mm
Filament density	1.25g/cm ³
Unsupported area threshold	50mm ²
Extra inflation distance	No
Bridging extension multiplier	100%
Bridging speed multiplier	100%

Advanced	
Layer modification	No
Slicing behavior	Heal
Gap fill when necessary	Yes
Percent overlap	Allow 10%
Only retrace when crossing open spaces	Yes
Force retraction between layers	Only for outermost perimeter

Table 1 – Table of Simplify3D settings used to print each conduit. Bolded words represent categories in the options menu.

Bibliography

- Alajmi, A., & Grader, A. (2009). Influence of fracture tip on fluid flow displacements. *Journal of Porous Media*, 435-447.
- Baraka-Lokmane, S., Main, I., Ngwenya, B., & Elphick, S. (2007, November). Application of complementary methods for more robust characterization of sandstone cores. *Marine and Petroleum Geology*, 26, 39-56.
- Becker, M. W., Pelc, M., Mazurchuk, R. V., & Spornjak, J. (2003). Magnetic resonance imaging of dense and light non-aqueous phase liquid in a rock fracture. *Geophysical research letters*, 30(12), 48-1-48-4.
- Brunke, O., Neuber, D., & Lehmann, D. (2007). NanoCT: Visualizing of Internal 3D-structures. *Materials Research Society Symposium: Materials, Processes, Integration and Reliability in Advanced Interconnects for Micro- and Nanoelectronics*, 325-331.
- Cnudde, V., & Boone, M. N. (2013). High-resolution X-ray computed tomography in geosciences: A review of the current technology and applications. *Earth-Science Reviews*, 1-17.
- Dann, R., Turner, M., Close, M., & Knackstedt, M. (2011, July). Multi-scale characterisation of coastal sand aquifer media for contaminant transport using X-ray computed tomography. *Environmental Earth Sciences*, 63(5), 1125-1137.
- Dierberg, F. E., & DeBusk, A. T. (2005). An evaluation of two tracers in surface-flow wetlands. *Wetlands*, 8-25.
- Florea, L. J., Cunningham, K., & Altobelli, S. (2009). NMR imaging of fluid exchange between macropores and matrix in eogenic karst. *Ground Water*, 47(3), 382-390.
- George, M., & Abraham, T. (2007). pH Sensitive Alginate–Guar Gum Hydrogel for the Controlled Delivery of Protein Drugs. *International Journal of Pharmaceutics*, 123-129.
- Goldscheider, N., & Drew, D. (2007). Methods in Karst Hydrology. In N. Goldscheider, & D. Drew, *Methods in Karst Hydrology* (p. 3). Leiden: Taylor & Francis/Balkema.
- Gross, B. C., Erkal, J. L., Lockwood, S. Y., Chen, C., & Spence, D. M. (2014). Evaluation of 3D Printing and Its Potential Impact on Biotechnology. *Analytical Chemistry*, 3240-3253.
- Holzmer, F. J., Dwarakanath, V., Ewing, J. E., Jin, M., & Londergan, J. T. (2005). Characterization of tetrachloroethene DNAPL in low-permeability coastal plain sediments, North Carolina. *Environmental Engineering Geologists*, 197-208.
- Huling, S. G., & Weaver, J. W. (1991). *Ground Water Issue: Dense non-aqueous phase liquids*. Washington D.C.: United States Environmental Protection Agency.

- Huyakorn, P., Panday, S., & Wu, Y. (1994). A three-dimensional multiphase flow model for assessing NAPL contamination in porous and fractured media, 1. formulation. *Journal of Contaminant Hydrology*, 16(2), 109-130.
- Jakobsen, P. R., & Klint, K. E. (1999). Fracture distribution and occurrence of DNAPL in a clayey lodgement till. *Hydrology Research*, 285-300.
- Jancin, M., & Ebaugh, W. F. (2002). Shallow lateral DNAPL migration within slightly dipping limestone, southwestern Kentucky. *Engineering and Environmental Impacts of Karst*(2-3), 141-149.
- Lide, D., & Milne, G. (1994). *Handbook of Data on Organic COmpouds*. Boca Raton, FL: CRC Press.
- Loop, C., & White, W. B. (2001). A conceptual model for DNAPL transport in karst groundwater basins. *Ground Water*, 39, 119-127.
- Maggi, F. (2015). Experimental evidence of how the fractal structure controls the hydrodynamic resistance on granular aggregates moving through water. *Journal of Hydrogeology*, 694-702.
- MakerGear. (2017). *MakerGear M2 - Top-Rated Desktop 3D Printer - Makergear*. Retrieved from MakerGear: <https://www.makergear.com/products/m2>
- McCray, J. E., Tick, G. R., Jawitz, J. W., Gierke, J. S., Brusseau, M. L., Falta, R. W., . . . Wood, A. L. (2011). Remediation of NAPL source zones: lessons learned from field studies at Hill and Dover AFB. *Groundwater*, 49(5), 727-744.
- Moore, J. E. (2016, December). Personal Communication. Morgantown, West Virginia, USA.
- National Energy Technology Labs. (2013, November). NETL-ORD geoinaging characterization NETL's computed tomography (CT) scanners.
- Newell, C. J., Acree, S. D., Ross, R. R., & Huling, S. G. (1995). *Ground Water Issue: Light non-aqueous phase liquids*. Washington D.C.: United States Environmental Protection Agency.
- Palmer, A. N. (1991). Origin and Morphology of Limestone Caves. *Geological Society of America Bulletin*, 1-21.
- Polak, A., Elsworth, D., Yasuhara, H., Grader, A., & Halleck, P. (2003). Permeability reduction of a natural fracture under net dissolution by hydrothermal fluids. *Geophysical Research Letters*, 1-4.

- Russo, A., Mahal, M., & Brusseau, M. (2009, December). Non-ideal behavior during complete dissolution of organic immiscible liquid:1 natural porous media. *Journal of hazardous Materials*, 172(1), 208-213. b.
- Russo, A., Narter, M., & Brusseau, M. (2009). Characterizing pore-scale dissolution of organic immiscible liquid in a poorly-sorted natural porous medium. *Environmental Science and Technology*, 43(15), 5671-5678. a.
- Savla Associates. (2007). *photopolymer.com*. Retrieved November 16, 2016, from <http://www.photopolymer.com/stereolithography.htm>
- Singh, K., Niven, R. K., Senden, T. J., Turner, M. L., Sheppard, A. P., Middleton, J. P., & Knackstedt, M. A. (2011). Remobilization of residual non-aqueous phase liquid in porous media by freeze-thaw cycles. *Environmental Science and Technology*, 45(8), 3473-3478.
- Soga, K., Page, J., & Illangasekare, T. (2004). A review of NAPL source zone remediation efficiency. *Journal of Hazardous Materials*, 13-27.
- Toshiba Medical Systems Corporation. (2015). *ct-aq-one-fam-pop-up-brochure*. Retrieved from Medical.Toshiba.com: <https://medical.toshiba.com/download/ct-aq-one-fam-pop-up-brochure>
- USGS Office of Groundwater. (n.d.). *USGS Groundwater Issues::Karst::What is Karst?* Retrieved from USGS Groundwater Information: <https://water.usgs.gov/ogw/karst/pages/whatiskarst>
- V. Cnudde, M. B. (2013). High-resolution X-ray computed tomography in geosciences: A review. *Earth-Science Reviews*, 1-17.
- Weary, D. J., & Doctor, D. H. (2014). *Karst in the United States: A digital map compilation and database*. United States Department of the Interior, United States Geological Survey. Reston: USGS.
- White, W. B. (2002). Karst hydrology: Recent developments and open questions. *Engineering Geology*, 85-105.
- White, W. B. (2007). A brief history of karst hydrogeology: contributions of the NSS. *Journal of Cave and Karst Studies*, 13-26.
- Wildenschild, D., Vaz, C., Rivers, M., Christensen, B. S., Rickard, D., & Hopmans, J. (2002). Using X-ray computed tomography in hydrology: Systems resolutions and limitation. *Journal of Hydrology*, 285-297.

Worthington, S. R. (1999). A comprehensive strategy for understanding flow in a carbonate aquifer. In A. N. Palmer, M. V. Palmer, & I. D. Sasowsky (Ed.), *Karst Modeling* (pp. 30-37). Charlottesville: Karst Waters Institute.

zkus. (2016). Quality Finish 3D Prints with Acetone.